

# 1 Calibration of the MEMS v1 model over a continental soil 2 inventory: a comparison of MCMC and 4DEnVar methods

3 Toni Viskari<sup>1</sup>, Tristan Quaife<sup>2</sup>, Fernando Fahl<sup>1</sup>, Yao Zhang<sup>3</sup>, and Emanuele Lugato<sup>1</sup>

4 <sup>1</sup> European Commission, Joint Research Centre (JRC), Ispra, Italy

5 <sup>2</sup> National Centre for Earth Observation, Department of Meteorology, University of Reading, United Kingdom

6 <sup>3</sup> Natural Resource Ecology Lab, Colorado State University, USA

7 *Correspondence to:* Toni Viskari (toni.viskari@ec.europa.eu)

8  
9 **Abstract.** An abundant amount of different data is required to calibrate soil organic carbon (SOC) models to  
10 represent ecosystems at large-scale. However, due to challenges related to model state projections, this  
11 calibration becomes very computationally heavy with traditional calibration methods. Here, we test 4-  
12 Dimensional Ensemble Variational data assimilation (4DEnVar) method to parameterize the MEMS v1 SOC  
13 model using data from the LUCAS network and compare its performance against MCMC calibration.  
14 Additionally, we performed an experiment where we adjusted the litter input calculation to see if the two  
15 calibration methods react differently to the change. The total SOC projections from both parameterizations  
16 showed similar improvements though the produced parameter sets differed. A thorough analysis revealed that  
17 the detailed SOC states differed from each other, but we also lacked information to determine which parameter  
18 set was closer to the truth. Furthermore, changing the litter input partition highlighted how much that  
19 assumption affects the calibration results with both methods. Our results here establish 4DEnVar as an  
20 applicable calibration method for SOC models but also highlight the need for more nuanced validation methods,  
21 as well as careful examination on how different data sets affect the model calibration.

## 23 1 Introduction

24 Soil organic carbon (SOC) stocks are a major component of the global carbon cycle (Scharlemann et al., 2014)  
25 and are inherently linked to surface vegetation, as the long-term SOC compounds forming them are produced by  
26 decomposition of plant litter (Cornwell *et al.*, 2008). Due to the importance of those stocks, they are a central  
27 part of national carbon budgets (van den Berg et al., 2020) and targeted by climate related policy (e.g. LULUCF,  
28 CRCF; Schlamadinger et al., 2007) aiming at enhancing carbon accumulation into the soils and improve  
29 terrestrial carbon sinks (Rumpel et al., 2020). All of this has also highlighted the need to improve the current  
30 soil related Monitoring, Reporting and Verification (MRV) systems (Bellassen *et al.*, 2015).

31 Soil inventory and numerous measurement campaigns, both temporary and continuous, have been set up to  
32 actively observe the soil carbon states within given regions and/or ecosystems (Smith et al., 2020). While these  
33 provide valuable information about the SOC stocks in that time window, also utilizing faster sample collections  
34 and analysis (Loria *et al.*, 2024), they generally provide only information on the total SOC stocks.

35 To provide more nuanced SOC measurements, separating the bulk soil into SOC fractions (Cambardella and  
36 Elliot, 1992; Lavalley et al., 2019; Yu et al., 2022), notably the mineral-associated (MAOM) and the particulate  
37 organic matter carbon (POM), has been utilized more in current field campaigns. However, though there are  
38 different methods to measure these short- and long-lived SOC fractions (Delahaie et al., 2024), they require  
39 considerable resources to be applicable on a large spatial scale. Thus, models are a crucial tool in both providing  
40 more cost-effective estimates of SOC states across landscapes, as well as their responses to both climate and  
41 environmental changes.

42 To this purpose, numerous models of varying complexities have been developed (Chandel et al., 2023; Le Noë  
43 et al., 2023) with different approaches and focuses. Some are simple first-order dynamic models such as RothC  
44 (Coleman and Jenkins, 1996) while others are more complicated non-linear models such as MIMICS (Wieder et  
45 al., 2014) and Millennial (Abramoff et al., 2022). However, the lack of detailed information both regarding the

46 SOC state and drivers, such as litter and soil moisture, does affect the ability to reliably constrain the various  
47 processes included into the models. Therefore, it is necessary to calibrate the model with more measurements  
48 from different pedo-climatic and land cover conditions, in order to capture how they affect the SOC state. This,  
49 though, increases the computational cost of the calibration.

50 Additionally complicating matters is even when using spatially diverse data for calibration, there are numerous  
51 assumptions regarding how that driver data is applied within the model that will affect not just model forward  
52 projections, but also the calibration process itself. For example, NPP is commonly used as a proxy for litterfall  
53 in SOC models (e.g. Abramoff et al., 2022; Pierson et al., 2022), with empirical work showing that the approach  
54 is justified (Matthews, 1997). How this NPP should be divided between above- and belowground biomass and,  
55 consequently between different model pools, depends on the ecosystem (Jevon et al., 2022; Cao et al., 2024) and  
56 is critical for determining the soil litter input. Without much more detailed information than is often available,  
57 these NPP/litter related parameter cannot be simultaneously calibrated with the SOC model parameters because  
58 of how fundamentally those values are connected; increasing/decreasing the amount of soil litter will simply  
59 result in an increase/decrease in decomposition rates to fit the measured SOC values. While there are valuable  
60 additional measurement datasets such as 14C (Brunmayer et al., 2024) that can provide important additional  
61 constraints for determining effective litter inputs, even these are still affected by how the NPP input is presented  
62 to start with in the model. This is just one example of driver associated assumptions and a quick nimble  
63 calibration method is needed to assess how these uncertainties impact the calibration results.

64 The traditional grand standard for model calibration is the Monte Carlo Markov Chain Metropolis Hastings  
65 algorithm (MCMC; Geyer, 1992). This is a very computationally heavy approach with multiple variants having  
66 been developed over the years to make it more efficient in exploring the parameter space and avoid local  
67 likelihood maximas in its search for the most likely parameter sets (e.g Papaioannou et al., 2015; Vrugt, 2016).  
68 Due to the challenges discussed before, only computationally light SOC models can be calibrated within a  
69 practical time frame using large scale data (for example Tuomi et al., 2009). There have been workarounds  
70 presented, making assumptions about the initial state (Nemo, 2017; Mathers et al., 2023), using simpler  
71 calibration methods (Gurung et al, 2020) or taking advantage of machine learning approaches (Heuvelink et al.,  
72 2021). However, there remains a need for a fast and trustworthy calibration method for SOC models that would  
73 allow for easy experimentation on how different datasets affect the calibration or constraining new model  
74 dynamics being included. For example, equifinality is a known issue in ecosystem modelling, where there are  
75 multiple parameter sets that produce a similar model output (Sierra et al., 2015; Marschmann et al., 2019).  
76 Establishing if this is affecting the model system under study requires repeating the calibration multiple times  
77 which is prohibited by too heavy calibration approaches.

78 As a more practical alternative to the costly MCMC approach, four-dimensional ensemble variational data  
79 assimilation (4DEnVar; Liu et al., 2008) is a novel data assimilation approach, where a model ensemble  
80 generated by varying the parameters/variable states of interest is used to determine the optimal parameter and/or  
81 state variables. It has already been used for parameter calibration (Douglas et al., 2025; Pinnington et al. 2020)  
82 and is much faster than the traditional MCMC methods. It is based on the Four-dimensional Variational data  
83 assimilation (4DVar; Le Dimet and Talagrand, 1986), where a model projection is compared with observations  
84 and the new initial state for the next iteration is generated from this information. A key difference between  
85 MCMC and 4DVar based methods is that the latter use gradient descent methods to determine the next state  
86 instead of randomly sampling. While 4DVar has initially been used more commonly for state data assimilation,  
87 for example, in weather forecast (Huang et al., 2009), it has also been successfully applied to calibrate  
88 ecosystem models (e.g. Raoult et al., 2016; Peylin et al., 2016; Pinnington et al. 2016). However, to implement  
89 4Dvar with observations from multiple different times, an adjoint version of the model is needed which imposes  
90 its own challenges and limitations on the application (Thepaut and Courtier, 1991). The 4DEnVar method uses  
91 the ensemble to sidestep this requirement by simultaneously running multiple simulations with different  
92 parameter sets instead of an iterative solution. While to our knowledge there haven't been previous studies  
93 within the ecosystem modelling analysing the performance of the 4DEnVar to that of MCMC, in Beylat et al.  
94 (2025) the 4DEnVar method is compared to the original 4DVAR method in a very specific synthetic  
95 experiment. Within that scope the 4DEnVar was shown to be more effective than the original version, but it is  
96 only the first step in evaluation.

97 In the work presented here, we calibrated the MEMS v1 SOC model (Robertson et al., 2019) with both MCMC  
98 and 4DEnVar parameterization methods. The model in question simulates organic carbon decomposition

99 separately for above- and below-ground carbon with pathways from surface vegetation matter to the soil pools.  
100 In the framework of the MEMS v1, the microbial pool is the central connection between the different SOC  
101 states and, crucially, along with the soil properties regulates the amount of carbon stored as long-lived MAOM  
102 compounds. The SOC pools are for the most part connected by first order dynamics, but the relationship  
103 between the microbial and MAOM pool is non-linear. Consequently, there is only a small number of central  
104 parameters to calibrate while simultaneously the model steady state cannot be analytically solved, requiring the  
105 more costly parameterization process.

106 Soil data from the Land Use/Land Cover Area Frame Survey (LUCAS) measurement network (Orgiazzi et al.,  
107 2018) were used for calibration and validation against estimated model parameters, assessing their performances  
108 relative to each other and the default parameters. Because this LUCAS dataset contains measurements from  
109 thousands of plots across Europe and, thus, represents many different types of ecosystems as well as climate  
110 conditions, it allows to test a wider performance of the model calibration. One of the advantages was the level of  
111 standardisation in sample collection and analysis, the latter done by a unique laboratory, Furthermore, for a  
112 small subset of the chosen LUCAS dataset, the POM/MAOM fractioning also had been done, which provided  
113 more nuanced information for the calibration process. While Lucas is a standardised framework for SOC, was  
114 not specifically designed to assess the MAOM stocks.

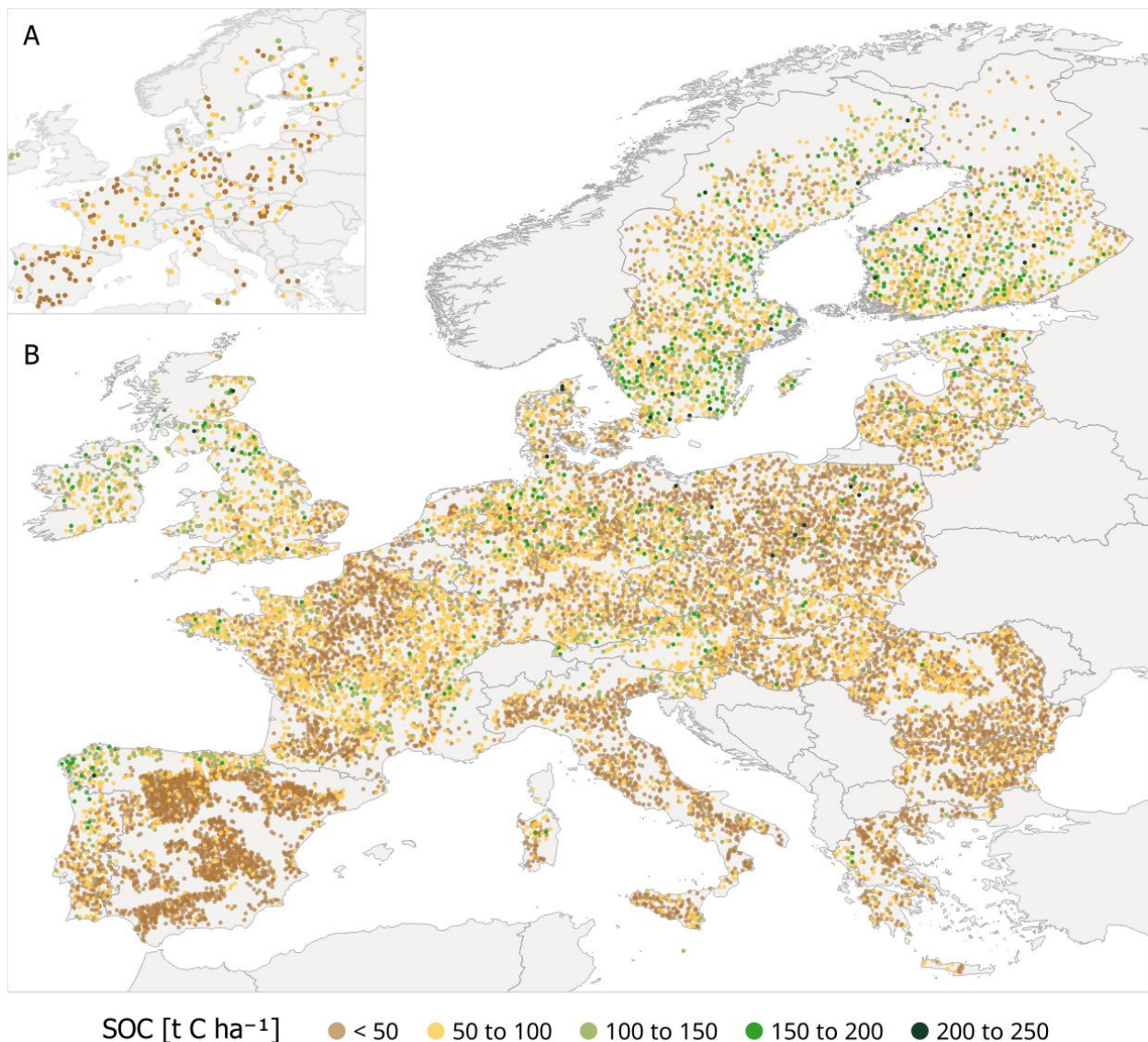
115 Our hypothesis is that the 4DEnVar improves the model fit to a sufficient degree that, along with the reduced  
116 computational cost, it can be considered as valid calibration approach for SOC models as the MCMC.  
117 Specifically, there are two objectives for the work presented here: the first is to test if the much faster 4DEnVar  
118 calibration performs as well as the MCMC calibration and examine if there are any meaningful differences in  
119 the resulting parameter sets; the second is to conduct a simple experiment where we made a change on how the  
120 NPP litter input was partitioned. The reasoning for the latter objective is that one of the core benefits of the  
121 faster calibration method is that it allows testing how different assumptions impact the parameterizations.  
122 Because of this, if there are differences between the results of the two calibration methods, it is important to  
123 assess if the general behaviour of the parameterizations remains the same even under different assumptions.

124

## 125 **2. Methods and data**

### 126 **2.1 LUCAS measurements**

127 For the model calibration, we used the LUCAS points from a field campaign conducted in 2009 as reported in  
128 Cotrufo et al., 2019 and Lugato et al., 2021. This dataset comprises; 1) the main physico-chemical characteristic  
129 of topsoil (0-20 cm), including total SOC content for about 20.000 samples distributed across different land  
130 covers in the EU and UK; 2) a size-fraction of the bulk SOC into mineral-associated (MAOM) and particulate  
131 organic matter carbon (POM) in a representative sub-set of 350 samples. The latter were randomly drawn from  
132 the all the measurements with the only constraint being that both datasets were similarly distributed across  
133 ecosystems with approximately 73 % being grass- or croplands with the rest being various forest types. Figure 1  
134 shows the LUCAS data points across Europe and the calculated SOC stock at each measurement site. The  
135 representativeness of the chosen 350 measurements points is elaborated upon in Lugato et al. (2021).



136

137 **Figure 1: The LUCAS 2009 sampling points across Europe and their SOC stock used for A) calibration and B)**  
 138 **validation.**

139 For the calibration, the 348 LUCAS measurements from the 2009 campaign containing POM/MAOM fractions  
 140 are used. The remaining 19 476 total SOC measurements were set aside for validation. In both allocations,  
 141 measurements which were not classified as agricultural, grassland or forest were removed as well as all the  
 142 sampling points where the driver data was not available. As a result, 322 datapoints are used for calibration and  
 143 17 430 for validation.

144 While the benefit of the LUCAS dataset is its large spatial representation and inclusion of measurements from  
 145 multiple different ecosystems, the execution of such a vast measurement campaign introduces different source  
 146 of errors from sampling, labelling, analysis etc. Thus, it is almost more apt to be considered as a combination of  
 147 several independent campaigns done with the same protocols, instead of a single consistently controlled  
 148 campaign. Additionally, although locations of the measurement are known, we have the make the assumptions  
 149 that the available driver data are representative for the actual conditions at the measurement plot.

150

## 151 **2.2 MEMS mode and parameters chosen for calibration**

152 The Microbial Efficiency-Matrix Stabilization V1 (referred to simply as MEMS for simplicity; Robertson et al.,  
 153 2019) model is a novel soil organic carbon (SOC) model framework, which is built around the scientific  
 154 understanding that the soil microbial pool modulates the SOC stocks. The model structure is presented in

155 Supplemental Figure 1. In the model, both surface vegetation and SOC decomposition are represented by  
 156 multiple pools defined by their physical properties. There are several paths for carbon fluxes to transfer from  
 157 one pool to another or lost as CO<sub>2</sub>, with the rate of change calculated on a daily timestep. The model dynamics  
 158 represents the depth of the soil measurements used to calibrate it. As we are using the LUCAS data here which  
 159 is from the top 20 cm of the soil, the resulting MEMS model will thus simulate the SOC dynamics of top 20 cm  
 160 layer as well.

161 Since the parameterization focuses on the SOC stock, only the model equations affecting MEMS pools C5  
 162 (Heavy particulate organic matter), C8 (Dissolved organic matter), C9 (Mineral associated organic matter  
 163 (MAOM)) and C10 (Light particulate organic matter) were calibrated here. The vegetation decomposition pools  
 164 C1 (hot-water soluble), C2 (acid soluble) and C3 (acid insoluble) as well as the surface microbial pool (C4) and  
 165 the dissolved organic matter (C6) do determine the litter input entering to soil C pools. These mechanics were  
 166 not included in the calibration as the type of data required to constrain them was not available. Therefore, we  
 167 used the default parameters values established in Robertson et al. (2019) for the surface processes since they had  
 168 been chosen to be representative of the LUCAS network environment. Meanwhile the released CO<sub>2</sub> (C7) and the  
 169 leached dissolved material to the soil (C11) are cumulative removal pools and do not have any parameters to be  
 170 calibrated.

171 The equations that govern the change in the relevant pools in MEMS are:

$$172 \quad \frac{dC_5}{dt} = C_{5,in}^2 + C_{5,in}^3 + C_{5,in}^4 - T_{mod}k_5C_5 \quad (1)$$

$$173 \quad \frac{dC_8}{dt} = C_{8,in}^5 + C_{8,in}^6 + C_{8,in}^{10} - sorp - DOC_{lch}C_8 - T_{mod}k_8C_8 \quad (2)$$

$$174 \quad \frac{dC_9}{dt} = sorp - T_{mod}k_9C_9 \quad (3)$$

$$175 \quad \frac{dC_{10}}{dt} = C_{10,in}^2 + C_{10,in}^3 - T_{mod}k_{10}C_{10} \quad (4)$$

176 Where  $C_i$  is the amount of carbon stored in pool  $i$ ,  $C_{i,in}^j$  is the carbon input to pool  $i$  from pool  $j$  as a result of the  
 177 decomposition process and  $k_i$  is the decomposition rate for pool  $i$ . The leaching coefficient  $DOC_{lch}$  represents  
 178 the dissolution of SOC to deeper soil layers and the temperature coefficient  $T_{mod}$  reflects how soil temperature  
 179 affects the decomposition rate. In this work,  $T_{mod}$  is the same for all pools and follows the STANDCARB 2.0  
 180 model (Harmon et al., 2009) which is an expanded version of the traditional Q10 temperature model where the  
 181 limiting impact of the high temperatures is accounted for.

182 The sorption coefficient  $sorp$  controls the flow of carbon between the microbial pool and the mineral associated  
 183 carbon pool as determined by the equation

$$184 \quad sorp = C_8 \frac{K_{lm}Q_{max}C_8 - C_9}{1 + K_{lm}C_8} \quad (5)$$

$$185 \quad Q_{max} = d \cdot \rho_{soil} \cdot (1 - p_{rock}) \cdot sc_{conc} \quad (6)$$

$$186 \quad sc_{conc} = sc_{slope} \cdot (1 - p_{sand}) + sc_{int} \quad (7)$$

187 In which  $K_{lm}$  is the langmuir isotherm term that depends on the soil pH,  $Q_{max}$  is the maximum absorption  
 188 capacity of the soil,  $\rho_{soil}$  is the soil bulk density,  $p_{rock}$  is the rock percentage of the soil and  $p_{sand}$  is the sand  
 189 percentage of the soil. The maximum concentration of fine fraction,  $sc_{conc}$ , is governed by the two coefficients  
 190  $sc_{int}$  and  $sc_{slope}$ . Consequently, those two parameters effectively control the saturation ratio for the MAOM  
 191 pool.

192 The decomposition rate parameters  $k_5$ ,  $k_8$ ,  $k_9$  and  $k_{10}$  were the central parameters chosen for calibration as well  
 193 as  $sc_{int}$  and  $sc_{slope}$ . As the primary focus of this work is to compare the calibration methods, these parameters  
 194 were simply chosen as a straight-forward test case. The boundary values are presented in Table 1. As will  
 195 explained in Section 2.5, we do need an expected value for these parameters in order to create a prior  
 196 uncertainty distribution. We chose this value by randomly drawing a parameter value from near the middle of  
 197 the set of the boundary conditions after testing that the model runs remained stable with these parameter values.

Name	Symbol	Expected value	Minimum value	Maximum value
Decomposition rate for heavy particle organic matter Pool (C5; day <sup>-1</sup> )	k <sub>5</sub>	0.0008	0.0001	0.002
Decomposition rate for dissolved soil organic material pool (C8; day <sup>-1</sup> )	k <sub>8</sub>	0.001	0.0001	0.01
Decomposition rate for mineral associated matter pool (C9; day <sup>-1</sup> )	k <sub>9</sub>	0.000025	0.00001	0.00004
Decomposition rate for light particle organic matter pool (C10; day <sup>-1</sup> )	k <sub>10</sub>	0.0005	0.0001	0.0004
Saturation intercept	SC <sub>Intercept</sub>	10.0	5	20
Saturation slope	SC <sub>Slope</sub>	0.25	0.1	0.4

198

199 **Table 1: The calibrated parameters chosen for calibration, their assigned expected parameter values as well as**  
200 **boundaries that constrain the lowest and highest values that the parameters are allowed be given during the**  
201 **calibration.**

202

203 To determine how we divide the litter input to MEMS model pools, the site ecosystem type was assigned by the  
204 Corine Land Cover (Buttner, 2014). Following that, NPP is split into the MEMS model pools according to the  
205 following framework established in Robertson et al. (2019):

$$206 \quad C_{1,input}(t) = (1 - f_{doc}^{eco})f_{sol}^{eco}r^{eco}NPP(t) \quad (8)$$

$$207 \quad C_{2,input}(t) = (1 - f_{sol}^{eco} - f_{lig}^{eco})r^{eco}NPP(t) \quad (9)$$

$$208 \quad C_{3,input}(t) = f_{lig}^{eco}r^{eco}NPP(t) \quad (10)$$

$$209 \quad C_{6,input}(t) = f_{sol}^{eco}f_{doc}^{eco}r^{eco}NPP(t) \quad (11)$$

210 Where  $C_{i,input}(t)$  is the carbon input to pool  $i$  from  $NPP$  at a given time  $t$  and  $eco$  refers to the ecosystem for the  
211 LUCAS point. Then,  $f_{sol}$  is the hot water extractable fraction of the litter input,  $f_{doc}$  is the cold-water  
212 extractable fraction of the water extractable fraction and  $f_{lig}$  is the acid-insoluble fraction of the of the litter  
213 input. It is important to note that these fractions are not the totality of the litter input and, while equations from 8  
214 to 11 do sum up to the total  $NPP$ , the fractions presented here do not sum up to 1. Finally, the  $r^{eco}$  represents the  
215 fraction of  $NPP$  that is assumed to have been removed from the system due to economic activities (harvest,  
216 grazing, etc.)

217 The coefficient values based on Campbell et al. (2016) are presented in Table 2. It is important to make two  
218 notes regarding these values. First, we are using a single fraction here and do not account for the uncertainty  
219 range provided in the work referenced. Second, only  $f_{sol}$  and  $f_{lig}$  fraction ranges are presented in Campbell et  
220 al., (2016). For  $f_{doc}$  we used a constant value across land covers in line with the work Robertson et al. (2019).

	NPP fraction ( $r^{eco}$ )	Hot water extricable fraction ( $f_{sol}$ )	Acid insoluble fraction ( $f_{lig}$ )	Cold water extricable fraction ( $f_{doc}$ )
Woody grassland	0.67	0.35	0.15	0.15
Pure grass	0.51	0.35	0.15	0.15
Sporadic grassland	0.59	0.35	0.15	0.15
Cropland	0.43	0.35	0.15	0.15
Mixture	0.77	0.375	0.295	0.15

Broadleaf	0.68	0.4	0.27	0.15
Conifer	0.78	0.35	0.32	0.15

221

222 **Table 2: The fraction of NPP that is used for litter input and how it is divided into different litter**  
 223 **compounds**

224

225

### 226 2.3 MCMC

227 Markov Chain Monte Carlo (MCMC; Geyer, 1992) is a widely used Bayesian model parameterization method.  
 228 The basis of this approach is straightforward: First values for the parameters chosen for calibration are drawn by  
 229 randomly perturbing accepted parameter values and the model is run for given locations with these parameters.  
 230 Assuming that the uncertainties are normally distributed, the total likelihood  $F$  of these projections, given  
 231 observations that correspond to model predictions, is calculated with

$$232 \quad F = \prod_{l=1}^{N_{obs}} (2\pi\sigma_l^2)^{-\frac{1}{2}} e^{-\frac{1}{2}\sum_{l=1}^{N_{obs}} \frac{(x_l - y_l)^2}{\sigma_l^2}} \cdot \prod_{k=1}^{N_{par}} (2\pi\sigma_{\theta,k}^2)^{-\frac{1}{2}} e^{-\frac{1}{2}\sum_{l=1}^{N_{par}} \frac{(\theta_k - \theta_{k,prior})^2}{\sigma_{\theta,k}^2}} \quad (12)$$

233 Where  $l$  is the observation index,  $N_{obs}$  is the number of observations,  $\sigma$  is the associated uncertainty,  $x_l$  is the  
 234 model projection with parameter set  $\theta$  and  $y_l$  is the observation for index  $l$ . Furthermore,  $k$  is the parameter  
 235 index,  $N_{par}$  is the number of parameters being estimated and  $\Theta_{prior}$  is the prior estimate of parameters.

236 Once the likelihood is determined, it is compared to the likelihood of the previously accepted parameter set. If  
 237 the new likelihood is higher, then that parameter set is automatically accepted and used as the parameters for the  
 238 next iteration. However, if the new likelihood is lower than the previous one, there is still a probability that the  
 239 new parameter set will still be accepted depending on how close the new likelihood is to the previous accepted  
 240 likelihood.

241 By allowing the lower likelihoods to be possibly accepted, MCMC also provides an acceptable parameter range,  
 242 which can be used to represent the parameter uncertainties. This iterative process is repeated until a given  
 243 convergence goal is satisfied (Roy, 2020).

244 For the study here, we used the MCMC framework established in Viskari et al. (2022), which utilizes the  
 245 BayesianTools R-library (Hartig et al., 2019). The chosen MCMC algorithm is the Differential evolution  
 246 Markov Chain with snooker updater (DEzs; ter Braak and Vrugt, 2008), where multiple calibration chains  
 247 progress concurrently from different starting point with information shared between the chains at given  
 248 intervals. This should lead to a more efficient and faster convergence of the calibration, especially as this  
 249 approach makes it possible to parallelize the different chains.

250 Six chains were used for the calibration with the initial values for each chain randomly drawn from the prior  
 251 parameter range. The MCMC was run for 100 000 accepted iterations with the convergence test and statistical  
 252 values calculated from the last 10 000 iterations.

253

### 254 2.4 4-Dimensional Ensemble Variational assimilation

255 Instead of iteratively exploring the variable space like MCMC does, 4-Dimensional Ensemble Variational data  
 256 assimilation (4DEnVar) uses an ensemble of model runs with different variable sets and that are independent of  
 257 each other. The ensemble of model runs is used to approximate information required by other calibration  
 258 techniques, such as the gradient of the cost function and a mapping from variable space to observation space.  
 259 Because there is no need for a large amount of model run repetitions such as in MCMC, this method is a  
 260 computationally much faster. However, this approach is built on certain assumptions – in particular that the  
 261 observations can be predicted by a linear combination of the different ensemble members - which make it  
 262 important to test before-hand how well it is able to find the correct values in different systems.

263 The foundational theory for the 4DEnVar method is explained in Liu *et al.* (2008). The formulation established  
 264 in Pinnington et al. (2020) was used as the basis for this work. In this section, we will provide a simplified  
 265 description of the method as it applies to our purposes.

266 In traditional baseline 4-Dimensional Variational data assimilation (4DVar; Le Dimet and Talagrand, 1986),  
 267 similarly to MCMC, the most likely state, i.e. the model parameter set, is solved by determining the minimum of  
 268 the cost function  $J$

$$269 \quad J = \frac{1}{2}((\boldsymbol{\theta} - \boldsymbol{\theta}_{prior})^T \mathbf{B}^{-1}(\boldsymbol{\theta} - \boldsymbol{\theta}_{prior}) + \sum_{t=1}^K (M_{0 \rightarrow t}(\boldsymbol{\theta}, \mathbf{x}_0) - \mathbf{y}_k)^T \mathbf{R}_t^{-1} (M_{0 \rightarrow t}(\boldsymbol{\theta}, \mathbf{x}_0) - \mathbf{y}_k)) \quad (13)$$

270 In which  $\boldsymbol{\theta}$  and  $\boldsymbol{\theta}_{prior}$  are, respectively, the suggested and prior parameter value vectors,  $\mathbf{B}$  is the prior  
 271 parameter error covariance matrix and  $\mathbf{R}_t$  is the observation error covariance matrix at the measurement time  $t$ .  
 272 The model operator  $M_{0 \rightarrow t}$  calculates from the given parameters and the initial state  $\mathbf{x}_0$  the output comparable to  
 273 the observation vector  $\mathbf{y}_k$ . The measurement times in the chosen time window is represented by  $K$ .

274 Two brief notes on this formulation. First, it is essentially the same as exponent component in Eq 12, except that  
 275 is written it in vector form. Second, in an effort to simplify the equations, we did not include an observation  
 276 operator component in the equations. All our observations are point measurements that can be directly compared  
 277 with the model output, hence a separate observation operator was unnecessary for our purposes.

278 4DVar, like MCMC, is also an iterative approach that calculates the cost function with different state vectors to  
 279 test if the cost function value decreases. However, with 4DVar, the iterations suggested after the first attempt are  
 280 not randomly drawn, but rather determined by the gradient function

$$281 \quad \nabla J = \mathbf{B}^{-1}(\boldsymbol{\theta} - \boldsymbol{\theta}_{prior}) + \sum_{t=1}^K \mathbf{M}_{0 \rightarrow t}^T \mathbf{R}_t^{-1} (M_{0 \rightarrow t}(\boldsymbol{\theta}, \mathbf{x}_0) - \mathbf{y}_k) \quad (14)$$

282 Where  $\mathbf{M}_{0 \rightarrow t}^T$  is the adjoint of the tangent-linear version  $\mathbf{M}_{0 \rightarrow t}$  of the model operator  $M$ .

283 The benefit of the gradient use is that it results in a value of zero for the state vector that produces the cost  
 284 function minimum. Thus, gradient descent techniques (Ruder, 2016) are able to use the information from the  
 285 gradient to efficiently locate the cost function minimum and the optimal state vector.

286 Naturally, there are challenges in applying this method. The core hurdle is the adjoint operator in equation Eq.  
 287 14, which is the transpose of the tangent-linear version of process model. Creating these model versions, though,  
 288 is not a simple task and imposes a linearity assumption on the driving processes. Furthermore, since background  
 289 error covariance matrix  $\mathbf{B}$  can have non-diagonal terms representing error covariances, the inverse matrix can  
 290 become computationally implausible to be calculated for larger systems.

291 In 4DEnVar, these issues are approached by expanding on the square root transform framework established in  
 292 Tippett et al, 2003. Let us have an ensemble of model runs where, in our case, every ensemble has a different  
 293 parameter set randomly drawn from the same baseline prior distribution. In the 4DEnVar formulation, this prior  
 294 distribution is assumed normally distributed. For each ensemble member, we can then determine how its output  
 295 differs from the prior parameter set output. These perturbations from the mean across the ensemble can be  
 296 written in matrix format  $\boldsymbol{\Theta}'_b$  as follows

$$297 \quad \boldsymbol{\Theta}'_b = \frac{(\boldsymbol{\theta}^{b,1} - \bar{\boldsymbol{\theta}}^b, \boldsymbol{\theta}^{b,2} - \bar{\boldsymbol{\theta}}^b, \boldsymbol{\theta}^{b,3} - \bar{\boldsymbol{\theta}}^b, \dots, \boldsymbol{\theta}^{b,L} - \bar{\boldsymbol{\theta}}^b)}{\sqrt{L-1}} \quad (15)$$

298 Where  $L$  is the ensemble size,  $\boldsymbol{\theta}^{b,i}$  is the  $i$ th vector of the perturbation matrix, and  $\bar{\boldsymbol{\theta}}^b$  is the average over the  
 299 perturbations. In our case, the average over the perturbations is the same as the prior parameter vector  $\boldsymbol{\theta}_{prior}$ .

300 Since this matrix essentially represents the uncertainty related to the parameter values, the prior error covariance  
 301 matrix  $\mathbf{B}$  can be approximated as

$$302 \quad \mathbf{B} \approx \boldsymbol{\Theta}'_b \boldsymbol{\Theta}'_b{}^T \quad (16)$$

303 We admit that in this formulation we ignore model structural error and assume the dominant error is from the  
 304 parameter uncertainty.

305 Furthermore, we can define a vector  $\mathbf{w}$  with the length of  $L$  that satisfies the equation

306  $\mathbf{w} = \boldsymbol{\Theta}'_b^{-1}(\boldsymbol{\theta} - \boldsymbol{\theta}_{\text{prior}})$  (17)

307 With these formulations and assumptions, the cost and gradient functions can be written as

308  $J(\mathbf{w}) = \frac{1}{2} \mathbf{w} \cdot \mathbf{w}^T + \frac{1}{2} \sum_{t=1}^K (\mathbf{M}_{0 \rightarrow t} \boldsymbol{\Theta}'_b \mathbf{w} + M_{0 \rightarrow t}(\boldsymbol{\theta}, \mathbf{x}_0) - \mathbf{y}_k)^T \mathbf{R}_t^{-1} (\mathbf{M}_{0 \rightarrow t} \boldsymbol{\Theta}'_b \mathbf{w} + M_{0 \rightarrow t}(\boldsymbol{\theta}, \mathbf{x}_0) - \mathbf{y}_k)$  (18)

309  $\nabla J(\mathbf{w}) = \mathbf{w} + \sum_{t=1}^K \boldsymbol{\Theta}'_b{}^T \mathbf{M}_{0 \rightarrow t}^T \mathbf{R}_t^{-1} (\mathbf{M}_{0 \rightarrow t} \boldsymbol{\Theta}'_b \mathbf{w} + M_{0 \rightarrow t}(\boldsymbol{\theta}, \mathbf{x}_0) - \mathbf{y}_k)$  (19)

310 With this new formulation, we can further approximate

311  $\nabla J(\mathbf{w}) = \mathbf{w} + \sum_{t=1}^K (\mathbf{M}_{0 \rightarrow t} \boldsymbol{\Theta}'_b)^T \mathbf{R}_t^{-1} (\mathbf{M}_{0 \rightarrow t} \boldsymbol{\Theta}'_b \mathbf{w} + M_{0 \rightarrow t}(\boldsymbol{\theta}, \mathbf{x}_0) - \mathbf{y}_k)$  (20)

312 This formulation removes the need for the adjoint version of the model. An additional benefit of the 4DEnVar  
 313 method is that the gradient function value can be calculated for each ensemble member, since we are already  
 314 running an ensemble to approximate the prior error covariance matrix. This information, then, makes  
 315 straightforward determining the state estimate.

316 Compared to filter-based data assimilation methods (for example the Ensemble Kalman Filter; Evensen, 2003),  
 317 the variational methods do not estimate the posterior uncertainty directly. However, we used the method  
 318 established in Pinnington et al. (2021) to calculate the posterior distributions.

319 For the study here, we used the 4DEnVar algorithm provided in Quaife (2023). The gradient approach method  
 320 used there is BFGS2 (Saito and Nakano, 1997) from the GNU Scientific Library (GSL).

321 The 4DEnVar methodology holds crucial benefits for our model calibration even beyond the reduction in  
 322 computational cost compared to MCMC. Even though all the measurements used for calibration in this work are  
 323 from the same year, the model outputs are steady state products that take hundreds of simulated years to  
 324 produce. Hence, a 3-dimensional variational data assimilation (3DVar; Lorenc et al., 2000) cannot be applied  
 325 and the adjoint of the model would be required, as the gradient function needs to be calculated at the start of the  
 326 simulation. To complicate things further, the validity of the tangent-linear assumption would be questionable  
 327 due to the length of the simulation in this situation.

328

## 329 2.5 Calibration setup and uncertainty attribution

330 After having set up the algorithmic framework for both calibration methods for the selected LUCAS data points,  
 331 the first task was to complete twin experiments. In those, we randomly drew a value for each the parameter  
 332 chosen for calibration from the uncertainty distributions assigned for them in Table 1. Synthetic observations  
 333 were generated with the model using the new parameter set. Then, we performed the calibration with both  
 334 tested methods using these synthetic observations with their associated uncertainties set to be 1 % of those  
 335 synthetic observations and still using the same prior distribution established in Table 1. This allows us to check  
 336 if both methods were able to find the correct parameter sets in a situation where the true answer was known. For  
 337 the 4DEnVar, the additional importance of these tests is to assess the ensemble size dimension required to  
 338 consistently estimate the correct parameter set. This was accomplished by repeating the twin experiment  
 339 multiple times with different ensemble sizes and choosing the ensemble size where the calibration always found  
 340 the correct parameter set. The repetitions were necessary because the 4DEnVar ensemble members are  
 341 randomly drawn, therefore there are potential situations where a given ensemble size can retrieve the correct  
 342 parameter set several times in a row, but then fails on the next time.

343 After the twin experiments have been conducted, the calibration itself is performed with the calibration dataset,  
 344 before the validation runs are done for the validation dataset locations. In both situations the SOC is assumed to  
 345 reflect a steady state. It should be noted that with agricultural soils and commercial forests are expected to have  
 346 a large variability in litter input over a given time window, which does raise challenges for the steady state  
 347 approach. We are still including those data points in the analysis here as this is intended as a general calibration  
 348 across European ecosystems and there is no additional data to constrain those specific ecosystems, but this is  
 349 expected to be an additional uncertainty source. As a part of the testing here, we also wished to experiment how  
 350 varying assumptions regarding model drivers affected the potential differences between the calibration results.  
 351 For our test case study on the impact of the NPP assumptions on the parameterization, we repeated the

352 calibrations with a small adjustment. We changed the  $f_{doc}$  value of grass- and croplands from 0.15 to 0.35. This  
353 increases the amount of the litter that is directly deposited to the soil and consequently adsorbed by the mineral  
354 matrix instead of being lost during the transition between the surface and soil carbon pools. In our expert  
355 opinion, there is a higher proportion of exudates and root litter (i.e. low molecule weight compounds that can  
356 directly sorbed by the soil minerals) entering the topsoil in grasslands and herbaceous compared to forests.  
357 Thus, this change is suitable for a plausible change to the NPP assumptions and makes an ideal test study to see  
358 how it affects the parameterization results and if the system depicted by the parameterizations still remains  
359 consistent after the potential change.

360 When calculating the steady state, the MEMS model is simulated over the period of 700 years from an initial  
361 state vector (Supplemental Table 1). Here, during calibration each LUCAS point is simulated for 700 years with  
362 the last output values compared to the measurements. At some sites, the MEMS model did not reach full steady  
363 state during this time, but the difference was within fractions of a percentage of the final steady state. As the  
364 change was so marginal already at this point, the shorter time period was chosen for computational efficiency.

365 As driver data at the European level, the model uses daily air temperature extracted from the E-OBS grid  
366 (Cornes et al., 2018). For each day of the year, an average temperature is calculated from a time series that spans  
367 from 2009-2018, with the temperature cycle then repeated for each year when calculating the steady state.  
368 Furthermore, the clay, sand and rock content of the soil as well as the soil bulk density and pH from LUCAS are  
369 used to determine soil properties driving SOC processes.

370 For Net Primary Production (NPP), first the average annual NPP over the decade 2000-2010 is extracted from  
371 the MODIS product MOD17A3 (Running et al., 2004) grid cell overlaying each LUCAS point. Then, a standard  
372 sine function is used to distribute the NPP across the year in order to produce the daily litter input. This  
373 approach was used instead of an averaged MODIS NPP annual time series as the NPP reflects the time when the  
374 atmospheric carbon is allocated into vegetation, not when the vegetation becomes litter input. Hence, we  
375 simplified the time series here and, since the total annual NPP remains the same, it is not expected to affect the  
376 modelling results to a notable degree.

377 The total SOC measurement uncertainties from the LUCAS dataset are used as the uncertainties in this  
378 application. Since LUCAS protocol requires to take a composite soil sample (out of 5 samples), the uncertainty  
379 was estimated propagating the error associated to all variables for calculating SOC stock (i.e. SOC content,  
380 depth, rock fragment). We run a Monte Carlo simulation with 5000 draws, using a standard deviation derived  
381 from the coefficient of variation reported in Goidts et al., 2009 for the microsite scale, with a similar sampling  
382 scheme of LUCAS. It is important to note, though, that these values are calculated from mixed samples. Thus, it  
383 may be an underestimation of the real uncertainty for several reasons as, for example, how LUCAS samples are  
384 overall representative of the field conditions. However, we do not have more information concerning the SOC  
385 measurement uncertainties available.

386 Regarding the MAOM fraction, there is no established uncertainty estimate to utilize. Because of that, we  
387 assigned an uncertainty where the standard deviation was 5 percent of the measured MAOM value. This choice  
388 was driven by both a discussion with the data collection team about the reliability of the data and to ensure an  
389 appropriate weight during the calibration process. When the initial cost function is calculated using the baseline  
390 MEMS parameter set with this uncertainty, the total SOC values account for approximately two thirds of the  
391 cost function value, with the MAOM fraction being responsible for the remainder.

392 The prior uncertainty assigned to the parameters introduced challenges in this work. With MCMC, because we  
393 only use the prior parameter value range for the initial sampling, we were able to apply a uniform uncertainty  
394 distribution that was used to approximate the baseline parameter set from Robertson et al., 2019. For those  
395 parameters where the uncertainty was not provided, we approximated a wide enough uniform distribution  
396 around the assigned parameter value. The 4DEnVar method, though, requires a Gaussian uncertainty  
397 distribution as explained in section 2.4. As there is no prior information available, we used the baseline  
398 parameter values as the expected values, with the uncertainty represented by a standard deviation of 10 % of the  
399 parameter value. This uncertainty range, deliberately imposing a larger uncertainty, resulted in 4DEnVar  
400 calibration producing negative parameter values, which are naturally unrealistic. We will discuss the reasons  
401 and implications of this behaviour later.

402 In some studies, for example, uncertainty has also been a parameter estimated with MCMC (Cailleret et al.,  
403 2020). Considering the meaningful unknowns regarding the uncertainty approximations, this would be a valid  
404 approach to be applied here. We did not estimate uncertainties for the initial MCMC/4DEnVar comparison, as  
405 varying the uncertainties might cause issues with the gradient approach methods and, consequently, would make  
406 it difficult to interpret the differences between the two. After the comparison, though, we did perform a MCMC  
407 calibration of MEMS, where we also estimated a scaling parameter for both total SOC and MAOM fraction  
408 uncertainties. However, these results are not shown here, as the calibration did not result in a successful  
409 convergence.

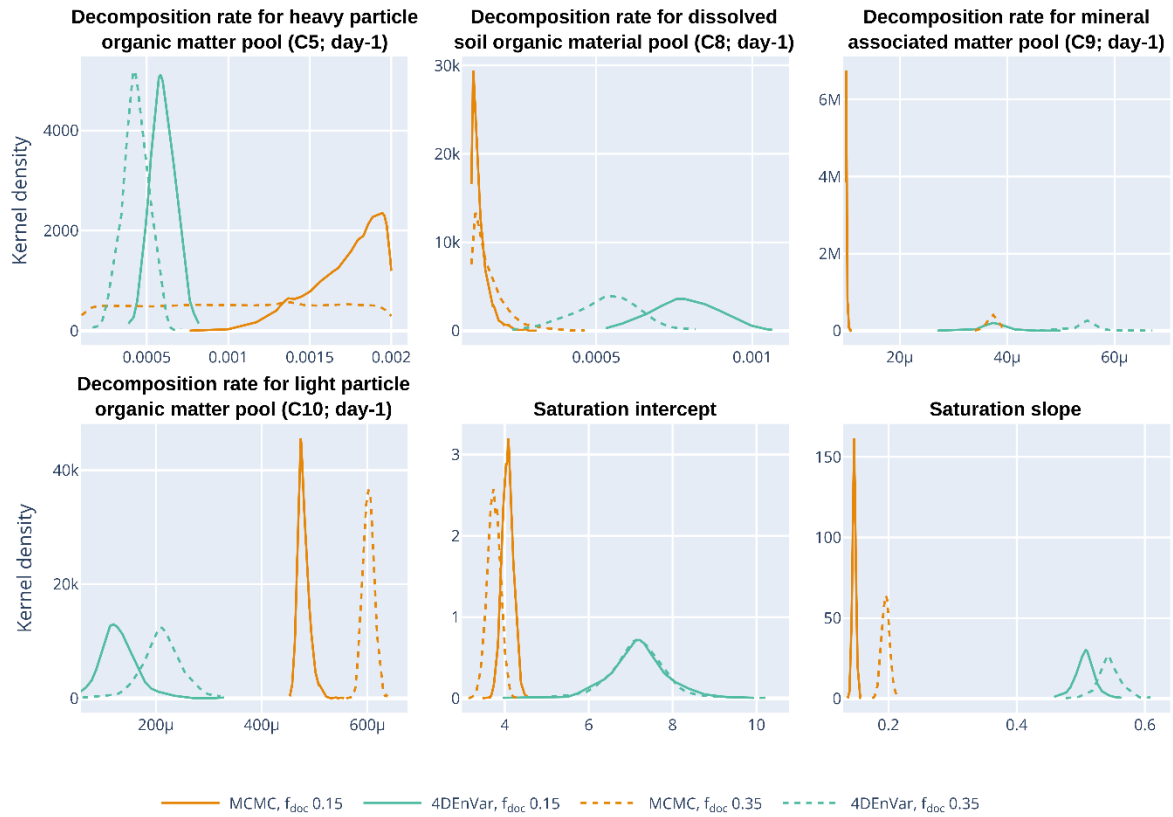
410

### 411 **3 Results**

412 The twin experiments (not shown) established that both methods were able to produce the true parameters when  
413 calibrating against synthetic observations. For 4DEnVar, the experiments established that an ensemble size of  
414 250 members consistently produced the parameters used to generate the synthetic observations for all repetitions  
415 of the twin experiment and, thus, we chose this ensemble size for the 4DEnVar consequents.

416 The parameter distributions estimated by the MCMC and 4DEnVar calibration for both  $f_{doc}$  scenarios are  
417 presented in Figure 2. For clarity, the statistically likeliest parameter values from all the calibrations are in Table  
418 3 and the standard deviations for the distributions in Supplemental Table 2. From these, we see that MCMC and  
419 4DEnVar parameter sets differ from each other more than explained by their associated uncertainties, but  
420 remain within the same range even when changing the NPP assumption. Furthermore, with the higher  $f_{doc}$   
421 value, the parameter distributions produced by 4DEnVar remain approximately as wide even when they shift.  
422 Meanwhile with the MCMC calibration it produces wider distributions which represents larger uncertainties. It  
423 is also apparent that with three parameters ( $k_8$ ,  $k_9$  and  $Sc_{slope}$ ), the MCMC produces expected values that are very  
424 close to the set boundaries when  $f_{doc}$  is set to 0.15 while, when set to 0.35, those distributions are clearly within  
425 the given parameter ranges. This indicates that with the lower  $f_{doc}$ , the MCMC calibration struggles to find an  
426 acceptable parameter set within the accepted range. Similarly, the uncertainties with the 4DEnVar are quite  
427 wide, which implies that it also cannot effectively locate an ideal parameter set.

428



429

430 **Figure 2: Estimated parameter distributions for both MCMC (orange) and 4DnVar (green) calibrations with  $f_{doc}$**   
 431 **set to 0.15 (solid) and 0.35 (dashed). The  $\mu$  indicates a multiplier of  $10^{-6}$ .**

432

433 The uncertainty distributions for 4DnVar are generally wider than for MCMC in both cases. With 4DnVar,  
 434 we repeated the calibration multiple times to ascertain that the randomness associated with the ensemble  
 435 selection did not result in statistically different parameter sets. While there was variance in the produced  
 436 parameter sets, they overall remained within the uncertainty distribution for any single estimation.

437

	4DnVar	MCMC
$k_5$	0.0006/0.00043	0.0019/0.0019
$k_8$	0.00078/0.00053	0.0001 /0.0001
$k_9$	0.000038/0.000055	0.00001/0.000037
$k_{10}$	0.00013/0.00021	0.00047/0.0006
$SC_{Icept}$	7.14/7.16	4.15/3.7
$SC_{Slope}$	0.51/0.54	0.144/0.197

438

439 **Table 3: The statistically likeliest parameter values produced by the different calibration methods. The first value is**  
 440 **for  $f_{doc}$  0.15, the second for  $f_{doc}$  0.35.**

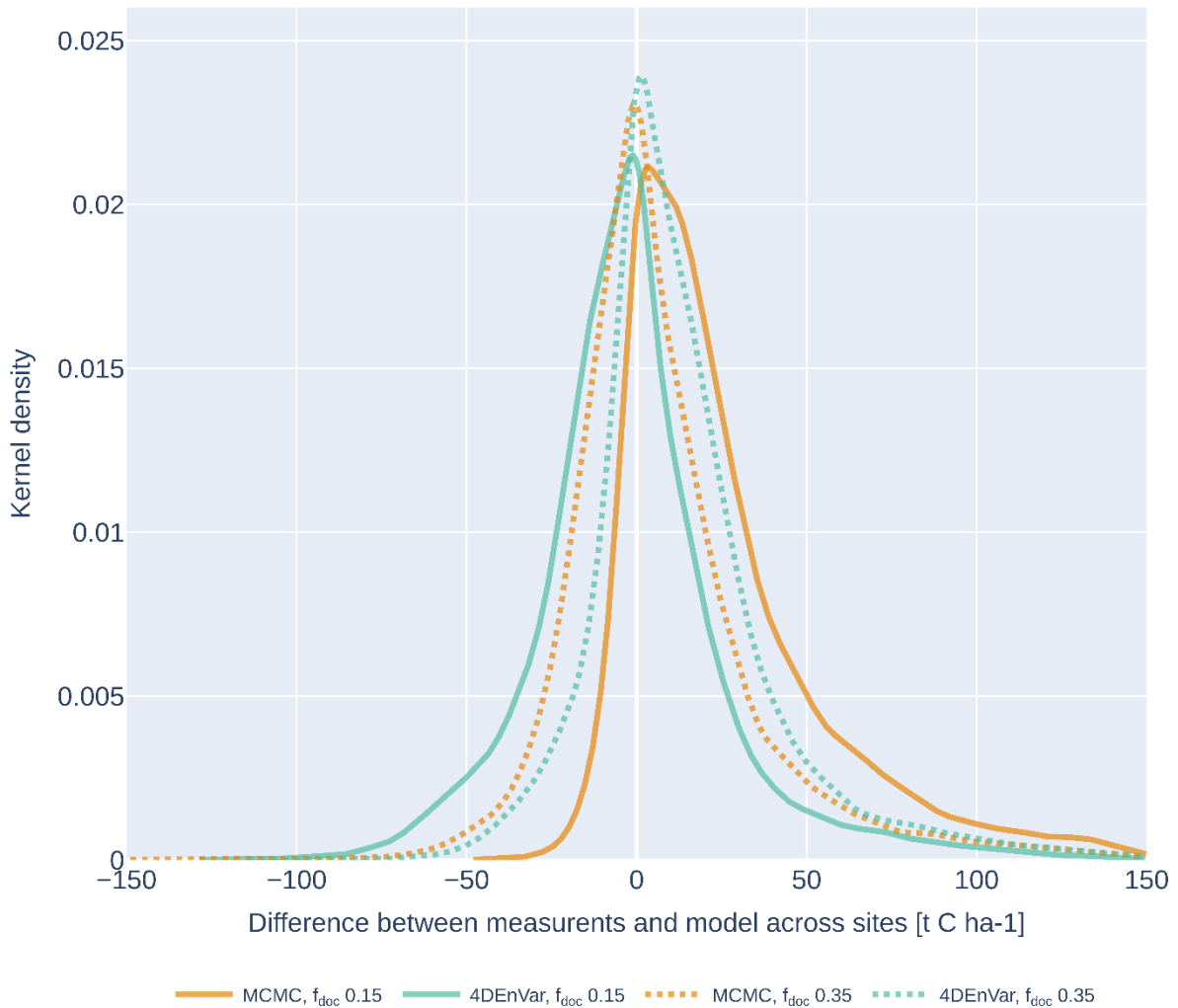
441 To examine the impact of the new parameter sets, Figure 3 presents the differences between the measurements  
 442 and model projections across all the validation sites, while Table 4 shows both the Root Mean Square Error  
 443 (RMSE) and mean error (ME) representing bias in regard of the validation dataset for each parameter set. While  
 444 the 4DnVar parameter sets produces a somewhat symmetric error distribution around zero in both calibrations,  
 445 with the higher  $f_{doc}$  there is a slight apparent tendency towards positive errors. In contrast, the MCMC error  
 446 distribution shows a notable lean towards positive errors for the lower  $f_{doc}$ , while with the higher  $f_{doc}$ , the bias  
 447 is much reduced. Since the SOC errors here are calculated as the measurement minus the model projection, this  
 448 means that positive errors reflect the parameter set systematically underestimating the SOC projections. It is

449 notable that with the higher  $f_{doc}$ , the RMSE values for the two parameterizations are very closer to each other  
 450 even with the larger positive bias of the 4DEnVar method.

	$f_{doc}$ 0.15	$f_{doc}$ 0.35
MCMC	42.5 / 27.4	31.3 / 7.4
4DEnVar	29.8 / -1.9	32.0 / 14.2

451

452 **Table 4: The error statistics for the different parameterizations with regard to the validation dataset. The**  
 453 **first value is for the root mean square error (RMSE) and the second for the mean error (ME). The unit**  
 454 **for all the values is t C ha<sup>-1</sup>.**



455

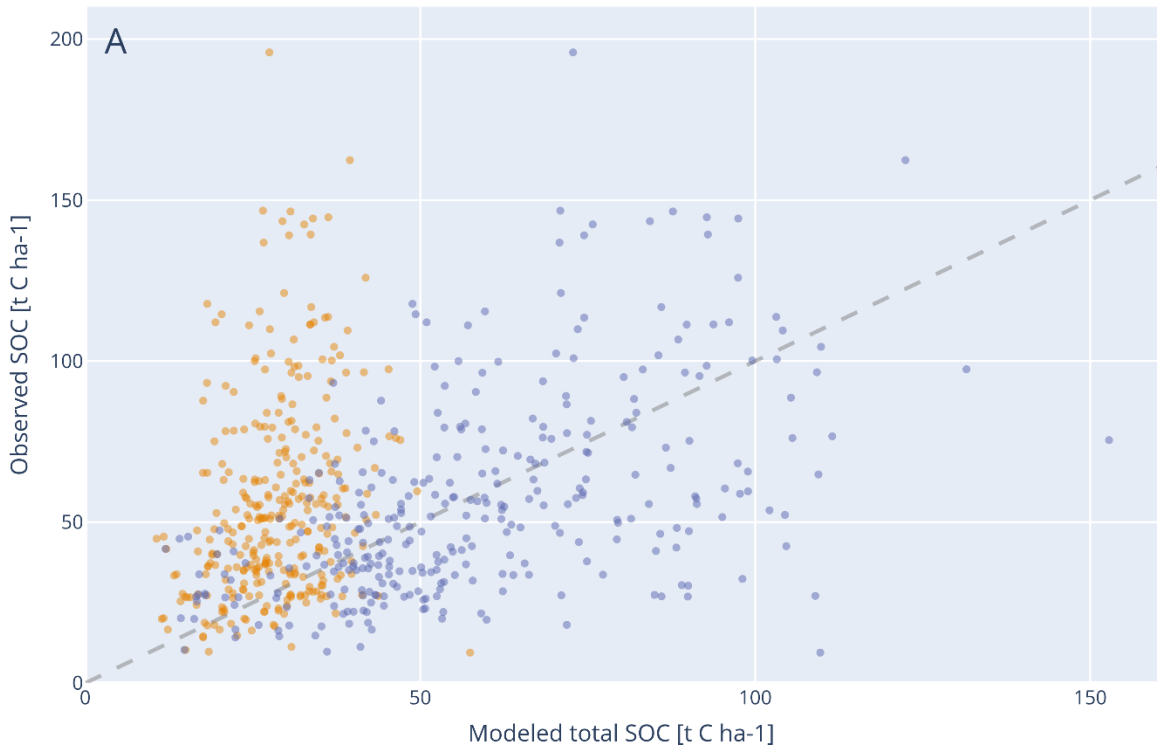
456 **Figure 3: The validation dataset error distributions for both MCMC (orange) and 4DEnVar (green) calibrations with**  
 457  **$f_{doc}$  set to 0.15 (solid) and 0.35 (dashed).**

458 To better comprehend what is causing the systematic MCMC error when  $f_{doc}$  is lower, we further examined the  
 459 actual calibration fit with both approaches in this scenario. Figure 4a shows how well the model SOC  
 460 projections follow the measurements and in Figure 4b the fit of the MAOM fraction with the 322 data points  
 461 used for calibration. From these comparisons, it is evident that, while the 4DEnVar parameter set follows the  
 462 measurement trend more closely than the MCMC, the latter calibration in turn replicates the MAOM:SOC  
 463 fraction much better. We also note that there are also clear biases as the 4DEnVar parameters constantly  
 464 underestimate the MAOM:SOC fraction, while there is a similar systemic underestimation of the total SOC with  
 465 the MCMC parameters. When comparing the calibration fits for the higher  $f_{doc}$  (Supplementary Figure XXX),

466 the behaviour remains similar with calibration methods, although the differences between the measured and  
467 modelled values become smaller.

468 When analysing of the cost function ( $J$ ) for each estimated parameter set (Not shown), the MCMC calibration  
469 resulted in a lower  $J$  with the initial  $f_{doc}$  while, with the increased  $f_{doc}$  (i.e. from 0.15 to 0.35), the difference in  $J$   
470 between the two approached was much reduced. However, when further looking at both total SOC and MAOM  
471 fractions measurements in both cases, the 4DEnVar produces a better match with total SOC while, conversely,  
472 the MCMC parameter set results in a closer fit with the MAOM fraction (MAOM: SOC) data. If we tighten the  
473 prior uncertainty used in the calibration, the 4DEnVar produces a different parameter set, though even those  
474 new parameters do still result in lower MAOM fractions in the validation dataset projections.

475

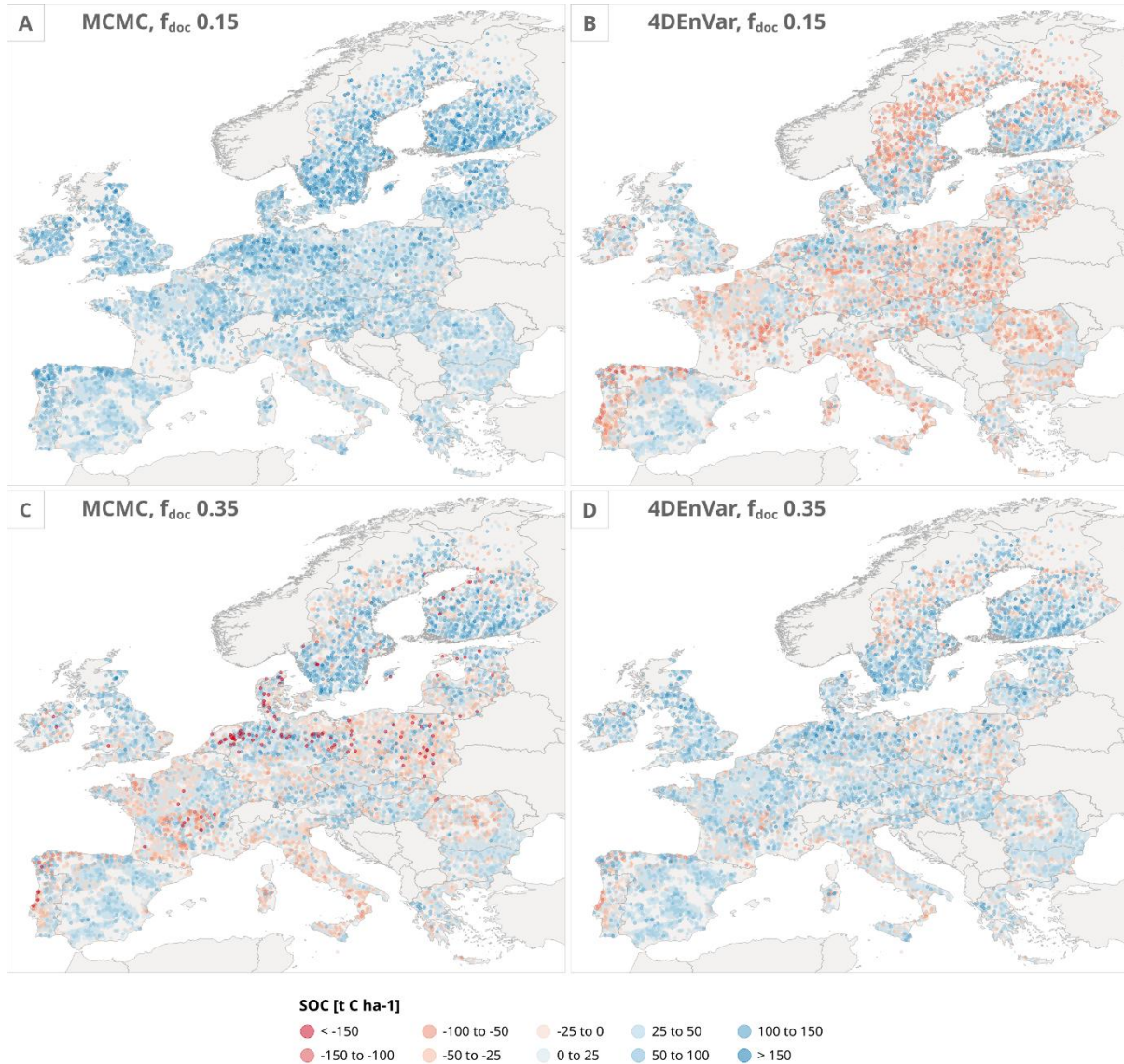


476

477 **Figure 4: For the calibration dataset, comparison between the modelled and measured a) Total SOC value and b)**  
 478 **MAOM:SOC fraction for both the MCMC and 4DENVar calibrations when  $f_{doc}$  was set to 0.15.**

479 Figure 5 shows the spatial distribution of the errors in Europe for both the MCMC and 4DEnVar parameter sets.  
 480 In the case of the lower  $f_{doc}$ , the MCMC underestimation is evident across Europe and, while the 4DEnVar map  
 481 is more evenly distributed, there are also clearly more local overestimations than when  $f_{doc}$  is set higher. In the  
 482 latter case, decrease in error can be seen across the whole Europe, with only a few clear areas, such as Nordic  
 483 countries and the Iberian Peninsula, with consistent bias in the error. However, what is intriguing is that across  
 484 central Europe, the prominent error points mirror each other. Where the MCMC parameter set produces  
 485 overestimations, the 4DEnVar parameter set conversely results in underestimations.

486



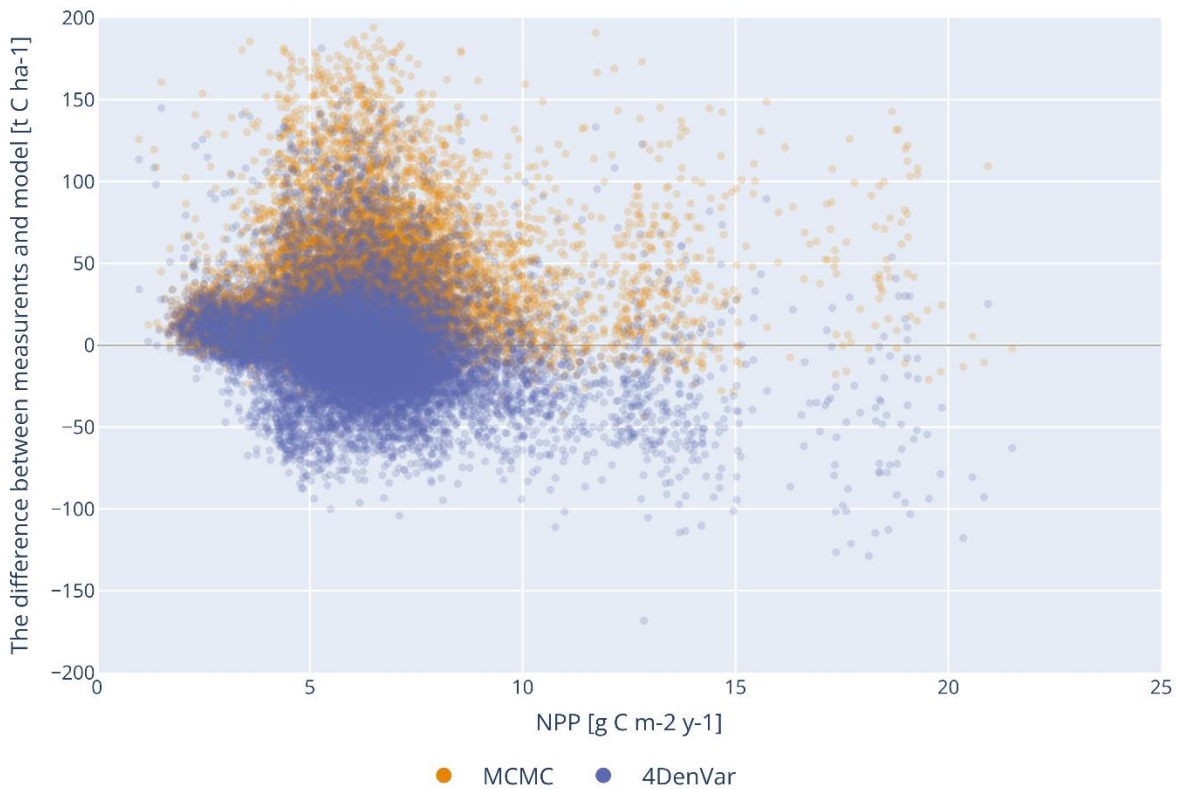
487

488

489 **Figure 5: Spatial error distributions across the LUCAS validation sites for a) MCMC with  $f_{doc}$  value of 0.15, b)**  
 490 **4DEnVar with  $f_{doc}$  value of 0.15, c) MCMC with  $f_{doc}$  value of 0.35, and d) 4DEnVar with  $f_{doc}$  value of 0.35**  
 491 **parameter sets**

492 Because of the pronounced errors when  $f_{doc}$  is set to the lower value, we further examined the relationship of  
 493 the SOC error with the NPP used as an approximation of the total litter input (Figure 6). During this  
 494 examination, it becomes evident that especially the MCMC parameter set projected a SOC underestimation  
 495 clustered around low NPP values.

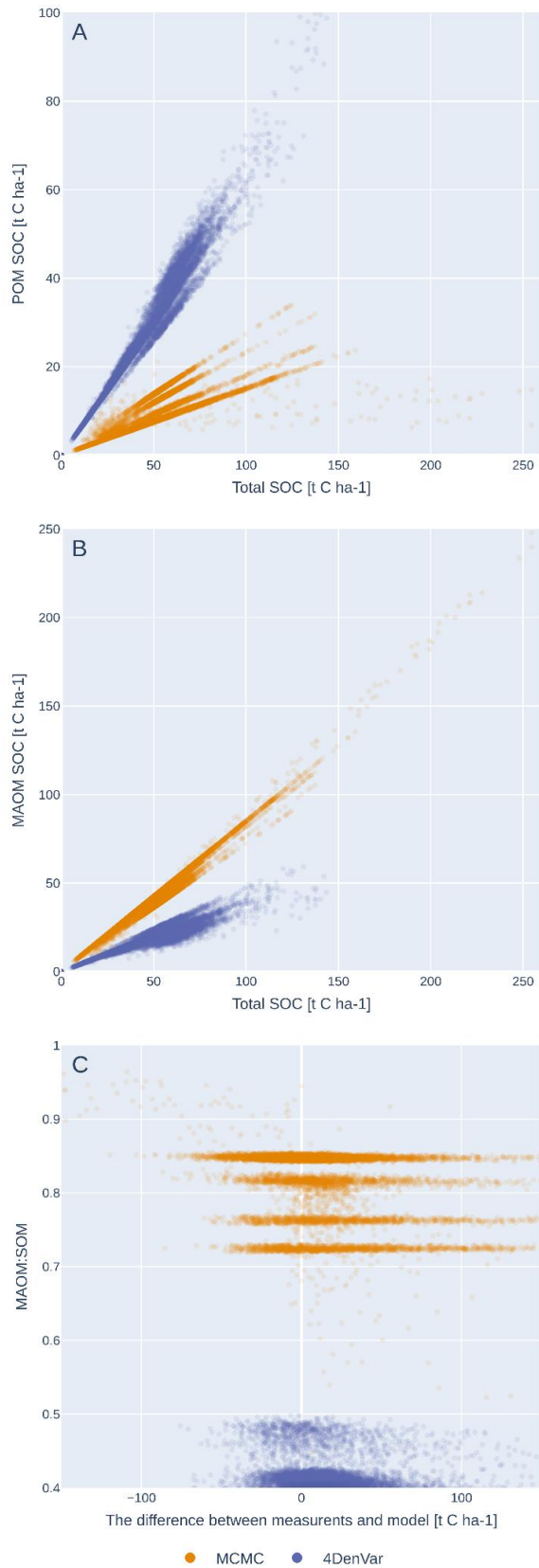
496



498

499 **Figure 6: Relationship between NPP and SOC projection error for both calibrated parameter sets after  $f_{doc}$  was set to**  
 500 **0.15**

501 Finally, we examined the POM, MAOM and MAOM:SOC fractions in relation to the total projected SOC stock  
 502 for the validation dataset with all calibrated parameter sets. Because of the systematic error when using the  
 503 lower  $f_{doc}$  and, due to the general behaviour remaining similar between the two scenarios, we are only  
 504 presenting the higher  $f_{doc}$  parameter set results here in Figure 7 for clarity. With the POM (Fig 7a) and MAOM  
 505 (Fig 7b), we can see similar differences between the two calibrations resulting from the initial calibrations. The  
 506 MCMC parameterization still produces much higher MAOM stocks than 4DenVar, and the latter  
 507 parameterization contrastingly results in higher POM stocks. Additionally, POM with MCMC parameters  
 508 remains at lower values than with the 4DenVar parameters while, for the 4DenVar parameters, MAOM hits a  
 509 ceiling sooner than for the MCMC parameters. To further examine the impact of these behaviours on the  
 510 projections, Figure 7c illustrates the relationship between the MAOM fraction and model error across all the  
 511 validation data points. Analysing the results further, we found that the very high SOC projections with both  
 512 MCMC and baseline parameters occurred in specific circumstances, where both NPP and annual temperatures  
 513 were low (not shown), and hence we attribute this to a structural issue within the model that arises in specific  
 514 conditions rather than the parameterization per se.



515

516 **Figure 7: The model projected a) POM, b) MAOM stocks in relation to the total modelled SOC stocks as well as c)**  
 517 **The MAOM:SOM ratio in relation to the model error across the LUCAS sites after  $f_{doc}$  was increased from 0.15 to**  
 518 **0.35.**

519

## 520 4 Discussion

### 521 4.1 Comparison between the performances of MCMC and 4DEnVar calibration methods

522 As seen in the results, the 4DEnVar approach is a straightforward tool for calibrating the MEMS v1 model with  
523 LUCAS data, as valid as the MCMC approach. Both had issues with the first parameterization attempt when it  
524 came to the validation dataset, but performed similarly when the direct litter fraction to soil was increased.  
525 Hence, the central problem with the first calibration attempt was not due to the calibration method itself. This  
526 supports 4DEnVar as a meaningful approach for initial calibration of soil carbon models, especially considering  
527 the massive difference in the required computational costs. For MCMC, the 100 000 iterations used here took  
528 over a month to compute on our HPC server while, simulating the 250 ensemble members without using  
529 parallelization, took approximately four hours. It should be noted that the MCMC calibration did begin to  
530 converge to the final values already after 40 000 iterations, but there is a risk in accepting the local cost function  
531 minima after such a relatively short calibration cycle. The computational cost for calibration from having to  
532 spin-up to steady state is a known issue with land system models in general (Raoult et al., 2025).

533 What is striking, though, is how much the parameter sets produced by the two calibration methods in both litter  
534 distribution scenarios differ from each, even with the higher  $f_{doc}$ , they perform approximately equally well with  
535 regard to the total SOC measurements in the validation dataset. As mentioned in the Introduction, equifinality, a  
536 situation where there exists multiple parameter sets that produce similar model outputs, is a known issue in  
537 ecosystem modelling and is evidently represented by the results here. The notable element here is that the  
538 calibration method itself determines the resulting parameter set as even when repeated, the MCMC calibration  
539 approach does not suggest the solution is in the same part of the parameter space as the 4DEnVar results  
540 indicate. Generally, twin experiments are efficient first pass to test for equifinality and the challenge can be  
541 addressed by reducing the amount of parameters being calibrated, but here there are questions how much those  
542 efforts can be relied on in assessing equifinality.

543 While we are not certain of what is driving these systematic differences between calibration sets, we  
544 hypothesize that one crucial component is that the total SOC and MAOM fraction measurements appear to  
545 incentivize contradicting model behaviours. Our twin experiment results support this theory as, with synthetic  
546 datasets, we were able to retrieve the same parameter set of both total SOC and MAOM that internally coherent  
547 with the model dynamics. This tension is especially evident when the  $f_{doc}$  is lower and there is less litter to  
548 distribute between the SOC pools. In that situation, MCMC is still able to find a solution by forcing a reduction  
549 in the decomposition rate for the MAOM pool and increasing the decomposition rate for the POM pool. This  
550 leads to a high MAOM fraction but at the cost of lower POM pool values and, consequently, a tendency to  
551 project lower SOC values. Meanwhile, this conflict between the two measurement types does seem to cause  
552 issues with the gradient approach method applied by 4DEnVar to determine the ideal parameter set. This could  
553 be because the disagreement between the data sources will create such a degree of noise in the likelihood space  
554 that determining a correct gradient descent from a collection of ensembles will become much more challenging.  
555 Simultaneously, though, this vulnerability in the 4DEnVar could be exploited in future work to quickly test if  
556 different measurement types and drivers are compatible within the model framework.

557 These results further highlight the fundamental impact of the priors on the calibration results, especially with the  
558 4DEnVar approach, that has been recognized as a larger challenge in ecosystem modelling (Dietze, 2017).  
559 While experimenting with the initial setup, we found that the 4dEnVar calibration produced unrealistic  
560 parameter values with negative decomposition rates, if prior was set to be too loose. This remained true even  
561 when increasing the  $f_{doc}$  value, although then the uncertainty could be loosened slightly more. Our hypothesis is  
562 that, while the MCMC iterative approach allows setting boundaries for the region where the values are sampled,  
563 such hard constraints are not present with the 4DEnVar. Additionally, the 4DEnVar does rely on the first order  
564 Taylor expansion, making it vulnerable to non-linear behaviours. Thus, incongruities resulting from missing  
565 model processes such as soil moisture, for example, can drive the parameterization beyond acceptable values if  
566 there is not a sufficient prior constrain implemented. This could be a partial explanation for the Iberian  
567 Peninsula error biases visible in Fig 5 as the soil moisture dynamics are much more complicated in arid climates  
568 vulnerable to drought (Almendra-Martin et al., 2021). A further limitation is that the 4DEnVar algorithm used  
569 here draws the ensemble members by sampling the prior distribution. While this is a logical approach when  
570 those distributions are reliably approximated, here we do not know what the prior distributions are and must use  
571 a tight uncertainty range in order to avoid unrealistic estimations. Consequently, our application of 4DEnVar  
572 samples the parameter space in a more limited manner than would be preferable.

573 The lack of knowledge on prior distributions for the parameters is an obstacle that is further hindered by the lack  
574 of reliable measurement uncertainty estimates. An important aspect of Bayesian statistics is that the weight of an  
575 individual information source depends on how accurate it is in comparison to the other available information  
576 sources. Hence, the width of the prior uncertainty that we can assign to constrain the parameter estimate to  
577 remain in a reasonable range is dependent on the measurement uncertainty. In this work, those uncertainties  
578 were so low that we had to use a relatively narrow prior parameter range for the 4DEnVar approach.  
579 Furthermore, as detailed in the Methods section, we do not have reliable approximations of the measured  
580 MAOC:SOC fraction uncertainties. Their uncertainty here is, thus, defined by how much weight we wished to  
581 give them in relation to the total SOC measurements. When we tested a larger measurement error, which in turn  
582 allowed us to increase the prior parameter distribution for the 4DEnVar without producing unrealistic estimates,  
583 the 4DEnVar ensembles also changed with the new values moving farther away from the baseline values. The  
584 implication is that the 4DEnVar is much more sensitive to the measurement uncertainty representation than  
585 MCMC, due to how the prior constraint is applied.

586 Naturally this underlines the overall importance of providing reliable measurement uncertainties along with  
587 measurements themselves, but that is not something a model user can simply produce by themselves. When  
588 implementing the calibration, based on the results here we would recommend of initially looking through the  
589 calibration data and confirming that all the values there are sensible for the model/system being calibrated. As a  
590 more practical solution, it is possible to repeat the 4DEnVar calibration multiple times by using the previous  
591 posterior distributions as the priors to the next cycle. This way it is possible to ensure that the resulting  
592 parameter set is not simply because the prior had been set too far from the correct value and thus partially  
593 reduce the impact of the assigned prior distribution. However, the downside of repeating the calibration cycle in  
594 this manner is that not only does it reduce the impact of the prior, but each iteration reduces the resulting  
595 uncertainty distribution. Thus, the final parameter distributions would be artificially too confident. While the  
596 repeated calibration is a worthwhile tool in certain circumstances, it always needs to be implemented with great  
597 care and consideration.

598

#### 599 **4.2 The impact of the NPP assumption on the calibrated parameter set performance**

600 Our results clearly underline how the fundamental assumptions regarding the NPP, as a litter proxy, impact the  
601 model calibration results. The lower  $f_{doc}$  resulted in a noticeable bias on total SOC predictions, especially with  
602 regard to the MCMC calibration. Another encouraging aspect of the work is that the differences between the  
603 two calibration methods results remain consistent even when changing the litter input assumption. This supports  
604 the capability of using the quicker 4DEnVar calibration to explore the impact of the NPP assumptions on the  
605 parameterization as any signal noted there should be reflected also in MCMC results.

606 What complicates future work is that coefficients associated with litter input are challenging to calibrate  
607 simultaneously with parameters associated with SOC decomposition, as their influence on the SOC overlap too  
608 much. It is important to note that while the focus in this experimentation has been the  $f_{doc}$  value, what it actually  
609 represents is the assumption of dividing NPP between upper- and below ground biomass as it reflects the  
610 amount of litter deposited directly into the soil. This is a central assumption that has to be included in some  
611 manner in SOC modelling and is represented by the plant species traits assigned to the surface vegetation. This  
612 highlights why better understanding of the vegetation qualities of the ecosystem being modelled is important for  
613 calibrating even simple SOC models.

614 As for even attempting to calibrate the NPP/litter coefficients simultaneously would first necessitate determining  
615 which exact coefficients would be calibrated. For example, in our case, there is first the question how well the  
616 MODIS NPP product represents reality for different systems. Then, part of that NPP is removed to represent  
617 economic activity before it is distributed to the four MEMS initial pools based on the three coefficients. Any of  
618 these three parts can be altered to change the final NPP input to the soil in different ways, but there is really no  
619 certainty at the moment what is the correct manner to better regulate the NPP based litter input. This  
620 complicated relationship in the surface vegetation driving litterfall and the SOC state has been shown in prior  
621 work such as in Raczka et al. (2021). There when they used remote sensing data to constrain their model state,  
622 while this improved their modelled aboveground biomass and carbon exchange accuracy, it also caused their  
623 modelled SOC accuracy to decrease because they were only using the aboveground data for both systems.

624 Adding to the challenges discussed above is that the various assumptions are not expected to be spatially  
625 homogeneous even in the same ecosystem type. For instance, the Nordic countries, especially Sweden and  
626 Finland, are dominated by economic forests where the NPP-to-litter pathway is heavily impacted by the growth  
627 stage as newly growing forest will have a large NPP, but not a corresponding amount of litter due to mortality.  
628 This could be connected to bias seen in the northern Europe in Fig 5. Another example would be agricultural  
629 ecosystems as climate conditions affect which crops will be dominant in a given region. The type of crops  
630 naturally affects its traits as, for instance, the root depth distribution, which in turn is expected to impact the soil  
631 carbon stocks (Fan et al., 2016). These various components could be a reason why when analysing global soil  
632 databases, there is a weak statistical relationship between NPP and SOC despite that dynamic being well  
633 understood (Luo et al., 2021). Naturally this is not to questioning the use of NPP as a litter input for soil carbon  
634 models. Rather it is another reminder on how important it is to be aware of the various assumptions related to  
635 the NPP and remain consistent with them while running the calibrated model in various systems. Additionally,  
636 when doing future SOC projections, the uncertainties related to the various NPP/litter assumptions should be  
637 considered during analysis.

638 The error distributions for both calibration methods when applying the higher litter input is in itself worthy of  
639 analysis. The MEMSv1 model used is lacking several dynamics that are known to impact soil carbon stock, such  
640 as soil moisture (Falloon et al., 2011), various nutrient cycles (Gardenas, et al., 2011; Feng et al., 2023) and  
641 mycorrhiza abundance (Hawkins et al., 2023). However, when considering the multitude of simplifications  
642 made to calculate the steady state approximations using parameters calibrated with data from 322 sites, the error  
643 distribution for the 17 000+ validation sites is much narrower than we initially expected. Which raises question  
644 how much of a further performance issue could be expected with addition of new processes? And, consequently,  
645 how can this limited data be used to evaluate which processes are most important for future projections?

646 Notably, while the spatial presentation of the model error under the higher  $f_{doc}$  shows only few regions where the  
647 differences between the two model errors are consistently larger than 10 tons of carbon per hectare, such as the  
648 Nordic countries, the MAOM fraction projections by the two model calibrations differ systematically to a  
649 meaningful degree. For instance, 4DEnVar calibration resulted in a higher turnover rate of the MAOM pool,  
650 which in turn causes lower MAOM stocks. Both calibration methods are adjusting the parameters to produce  
651 lower total SOC, as the baseline parameters tend to overestimate the SOC stocks, but they solve the issue with  
652 very different representations of the internal SOC state that would have a major impact on future projections.  
653 With the current available information, it is not possible to evaluate which of the two states is more realistic;  
654 while the MCMC modelled MAOM fractions are on average high for all ecosystems (Georgiou et al., 2022), the  
655 LUCAS dataset leans towards arable soils where the MAOM fraction is expected to be larger in the top layer  
656 than for forests (Schumpf et al, 2013; Sokol et al, 2022).

657 These outcomes emphasise the importance of carefully considering how model performance improvements are  
658 assessed with large-scale datasets such as the LUCAS measurement data, since the total SOC seems not  
659 sufficient which is in line with previous studies (Braakhekke et al., 2014; Guo et al., 2022). This is especially  
660 relevant as the model validation should be a crucial aspect of model choice regarding different SOC  
661 sequestration projects (Garsia et al., 2023). New measurement analysis methods allow for more efficient  
662 POM/MAOM fractioning of SOC samples (Delahaie et al., 2023), thus providing more detailed measurements  
663 to use during validation. However, as our results show, the SOC fractions might not be compatible with the total  
664 SOC measurements within the model context and indicate that there are missing processes within our model  
665 framework. Consequently, their value might be rather to evaluate what missing processes are needed within the  
666 model than validate existing parameterizations. Another approach for evaluation could be to examine the model  
667 performance within sub-regions or individual ecosystems instead of weighing it against the total dataset at once.  
668 A more nuanced approach to do this would be to use a hierarchical Bayesian approach (Gelman and Hill, 2007),  
669 but that requires more research on the applicability of that approach in solving the challenges highlighted by our  
670 results.

671

## 672 5 Conclusions

673 Calibrating soil organic carbon (SOC) models with large scale data sets is always a challenge due to the  
674 computational cost involved. Furthermore, numerous assumptions are made regarding model drivers that can  
675 potentially deeply affect the parameterization. In our work presented in this article, we have shown that

676 4DEnVar parameterization produces the approximately same RMSE for the validation dataset as the traditional  
677 and more cumbersome MCMC DEzs algorithm when the soil litter input is increased and actually outperforms  
678 in this metric the MCMC with the lower litter input. However, the parameter sets produced by the calibration  
679 methods differed from each other as did the model states they projected. Even though the total SOCs were  
680 similar, the difference between shorter lived POM and longer lived MAOM compounds was large enough to  
681 notably impact future projections. We also conducted a simple experiment to assess the impact of changing how  
682 the soil litter input is distributed among different litter pools. These results showed that while the litter input  
683 adjustment did impact the calibration, the general model behaviour produced by the two calibration methods  
684 remained similar. This implies, if it holds true with further testing, that the differences between the behaviours  
685 of the two calibration methods are not dependent on the driver data. Another facet of these results is that it  
686 confirms how large of an impact ecosystem related assumptions have on the resulting calibrations. The work  
687 here highlights how further consideration is required how to evaluate the model performances, especially on a  
688 larger scale. However, they also establish the fast 4DEnVar as a valid exploration tool that allows testing  
689 various scenarios with much more ease than the traditional MCMC approach. This will make it more  
690 pragmatically possible to assess how various assumptions impact ecosystem model results as well as better  
691 include those uncertainties in future projections as the various drivers are altered by climate change.

692

### 693 **Data/Code availability**

694 The MEMS v1 model version, the calibration algorithms as well as all the data used for calibration and  
695 validation is available on Zenodo at <https://doi.org/10.5281/zenodo.17314989> (Viskari et al. (2025)).

696

### 697 **Author contributions**

698 TV is the primary author of the manuscript and was responsible for creating the calibration framework as well  
699 as analysing the results. TQ provided expert assistance in implementing the 4DEnVar and insight into the  
700 results. FF helped setting up the environmental driver data and created the graphical presentation of the results.  
701 YZ is one of the creators the MEMS v1 model and offered expertise on prior calibration approaches with the  
702 model. EL is PI of the project that this research is a part of and was responsible for the LUCAS dataset model  
703 efforts.

704

### 705 **Competing interests:**

706 The authors declare that they have no conflict of interests.

707

### 708 **Acknowledgments**

709 This research was supported by the Carbon Removal on Land project, an administrative arrangement (n. 36662)  
710 between the Directorate-General Climate (DG-CLIMA) and the Joint Research Centre of the European  
711 Commission. Tristan Quaipe was funded under the International Programme of the UKRI National Centre for  
712 Earth Observation (NE/X006328/1).

- 713 References:
- 714 Almendra-Martin, L., Martinez-Fernandez, J., Gonzalez-Zamora, A., Benito-Verdugo, and Herrero-Jimenez,  
715 C.M.: Agricultural Drought Trends on the Iberian Peninsula: An Analysis Using Modeled and Reanalysis Soil  
716 Moisture Products. *Atmosphere*, 12(2), 236, 10.3390/atmos12020236, 2021
- 717 Abramoff, R.Z., Guenet, B., Zhang, H., Georgiou, K., Xu, X., Viscarra Rossel, R.A., Yuan, W., And Ciais, P.:  
718 Improved global-scale predictions of soil carbon stocks with Millennial Version 2. *Soil Biol Biochem*, **164**,  
719 108466, 2022
- 720 Bellassen, V., Stephan, N., Afriat, M., Alberola, E., Barker, A., Chang, J.-P., Chiquet, C., Cochran, I., Deheza,  
721 M., Dimopoulos, C., Foucherot, C., Jacquier, G., Morel, R., Robinson, R., and Shishlov, I.: Monitoring,  
722 reporting and verifying emissions in the climate economy. *Nature Climate Change*, **5(4)**, 319-328, 2015
- 723 Beylat, S., Raoult, N., Bacour, C., Douglas, N., Quaiife, T., Bastrikov, V., Rayner, P.J., and Peylin, P.: Towards  
724 the assimilation of atmospheric CO<sub>2</sub> concentration data in a land surface model using adjoint-free variational  
725 methods. *Geosci Model Dev*, **18**, 7501-7527, 10.5194/gmd-18-7501-2025, 2025
- 726 Braakhekke, M.C., Beer, C., Schrumppf, M., Ekici, A., Ahrens, B., Hoosbeek, M.R., Kruijtt, B., Kabat, P., and  
727 Reichstein, M.: The use of radiocarbon to constrain current and future soil organic matter turnover and transport  
728 in a temperate forest. *J Geophys Res Biogeosciences*, **119(3)**, 372-391, 10.1002/2013JG002420, 2014
- 729 Brunmayer, A.S., Hagedorn, F., Moreno Duborgel, M., Minich, L.I., and Graven H.D.: Radiocarbon analysis  
730 reveals underestimation of soil organic carbon persistence in new-generation soil model. *Geosci Model Dev*, **17**,  
731 5961-5985, 2024
- 732 Buttner, G: "CORINE land cover and land cover change products." In *Land use and land cover mapping in*  
733 *Europe: practices & trends* (pp. 55-74). Dordrecht: Springer Netherlands
- 734 Cailleret, M., Bircher, N., Hartif, F., Hulsmann, L., and Bugmann, H.: Bayesian calibration of a growth-  
735 dependent tree mortality model to simulate the dynamics of European temperate forests. *Ecol Appl*, **30**, e02021,  
736 10.1002/eap.2021, 2020
- 737 Cambardella, C.A., and Elliot, E.T.: Particulate Soil Organic Matter Changes across a Grassland Cultivation  
738 Sequence. *Soil Sci Soc Am J*, **56(3)**, 777-783, 1992
- 739 Campbell, E.E., Parton, W.J., Soong, J.L., Paustian, K., Hobbs, N.T., and Cotrufo, M.F.: Using litter chemistry  
740 controls on microbial processes on partition litter carbon fluxes with Litter Decomposition and Leaching  
741 (LIDEL) model. *Soil Biol Biochem*, **100**, 160-174, 2016
- 742 Cao, J., Li, Y., Biswas, A., Holden, N.M., Adamowski, J.F., Wang, F., Hong, S., and Qin, Y.: Grassland  
743 biomass allocation across continents and grazing practices and its response to climate and altitude. *Agric For*  
744 *Met*, 356, 110176, 10.1016/j.agrformet.2024.110176, 2024
- 745 Coleman, K., and Jenkinson, D. S.: RothC-26.3-A Model for the turnover of carbon in soil. In *Evaluation of soil*  
746 *organic matter models: Using existing long-term datasets* (pp. 237-246). Berlin, Heidelberg: Springer Berlin  
747 Heidelberg, 1996
- 748 Cornes, R.C., Van Der Schrier, G., Van Den Besselaar, E.J., and Jones, P.D.: An ensemble version of the E-  
749 OBS temperature and precipitation data sets. *J Geophys Res*, **123(17)**, 9391-9409, 2018
- 750 Cornwell, W. K., Cornelissen, J. H. C., Amatangelo, K., Dorrepaal, E., Eviner, V. T., Godoy, O., Hobbie, S. E.,  
751 Hoorens, B., Kurokawa, H., Perez-Harguindeguy, N., Quested, H. M., Santiago, L. S., Wardle, D. A., Wright, I.  
752 J., Aerts, R., Allison, S. D., van Bodegom, P., Brovkin, V., Chatain, A., Callaghan, T. V., Diaz, S., Garnier, E.,  
753 Gurvich, D. E., Kazakou, E., Klein, J. A., Read, J., Reich, P. B., Soudzilovskaia, N. A., Vaieretti, M. V., and  
754 Westoby, M.: Plant species traits are the predominant control on litter decomposition rates within biomes  
755 worldwide, *Ecol. Lett.*, **11**, 1065–1071, 2008.
- 756 Cotrufo, M.F., Ranalli, M.G., Haddix, M.L., Six, J., and Lugato, E.: Soil carbon storage informed by particulate  
757 and mineral-associated organic matter. *Nat Geosci*, **12**, 989-994, 2019

758 Delahaie, A.A., Barre, P., Baudin, F., Arrouays, D., Bispo, A., Boulonne, L., Chenu, C., Jolivet, C., Martin,  
759 M.P., Ratie, C., Saby, N.P.A., Savignac, F., and Cecillon, L.: Elemental stoichiometry and Rock-Eval® thermal  
760 stability of organic matter in French topsoils. *Soil*, 9, 209-229, 10.5194/soil-9-209-2023, 2023

761 Dietze, M.: Ecological forecasting. Princeton University Press. [10.1515/9781400885459](https://doi.org/10.1515/9781400885459), 2017

762 Douglas, N., Quaife, T., and Bannister, R.: Exploring a hybrid ensemble–variational data assimilation technique  
763 (4DEnVar) with a simple ecosystem carbon model. *Environmental Model Softw*, 106361, 2025

764 Evensen, G.: The ensemble Kalman filter: Theoretical formulation and practical implementation. *Ocean dyn*, **53**,  
765 343-367, 2003

766 Falloon, P., Jones, C.D., Ades, M., and Paul, K.: Direct soil moisture controls of future global soil carbon  
767 changes: An important source of uncertainty. *Glob Biochem Cycles*, **25(3)**, 10.1029/2010GB003938, 2011

768 Fan, J., McConkey, B., Wang, H., and Janzen, H.: Root distribution by depth for temperate agricultural crops.  
769 *Field Crops Res*, **189**, 68-74, 10.1016/j.fcr.2016.02.013, 2016

770 Feng, J., Song, Y., and Zhu, B.: Ecosystem-dependent responses of soil carbon storage to phosphorus  
771 enrichment. *New Phytol*, **238(6)**, 2363-2374, 10.1111/nph.18907, 2023

772 Gardenas, A.I., Agren, G.I., Bird, J.A., Clarholm, M., Hallin, S., Ineson, P., Katterer, T., Knicker, H., Nilsson,  
773 S.I., Nasholm, T., Ogle, S., Paustian, K., Persson, T., and Stendahl, J.: Knowledge gaps in soil carbon and  
774 nitrogen interactions – From molecular to global scale. *Soil Biol Biochem*, **43(4)**, 702-717,  
775 10.1016/j.soilbio.2010.04.006, 2011

776 Garsia, A., Moinet, A., Vazquez, C., Creamer, R.E., and Moinet, G.Y.K.: The challenge of selecting an  
777 appropriate soil organic carbon simulation model: A comprehensive global review and validation assessment.  
778 *Glob Change Biol*, 29(20), 5760-5774, 10.1111/gcb.16896, 2023

779 Gelman, A. and Hill, J.: Data analysis using regression and multilevel/hierarchical models. Cambridge  
780 University Press, Cambridge, 2007

781 Georgiou, K., Jackson, R.B., Vinduskova, O., Abramoff, R.Z., Ahlstrom, A., Feng, W., Harden, J.W.,  
782 Pellegrini, A.F.A., Polley, H.W., Soong, J.L., Riley, W.J., and Torn, M.S.: Global stocks and capacity of  
783 mineral-associated soil organic carbon. *Nat Commun*, **13**, 3797, 2022

784 Geyer, C.J.: Practical Markov Chain Monte Carlo. *Stat Sci*, **7(4)**, 473-483, 1992

785 Goidts, E., van Wesemael, B., and Crucifix, M.: Magnitude and sources of uncertainties in soil organic carbon  
786 (SOC) stock assessment at various scales. *Eur J Soil Sci*, **60**, 723-739, 10.1111/j.1365-2389.2009.01157.x, 2009

787 Guo, X., Viscarra Rossel, R.A., Want, G., Xiao, L., Wang, M., Zhang, S., and Luo Z.: Particulate and mineral-  
788 associated organic carbon turnover revealed by their long-term dynamics. *Soil Biol Biochem*, **173**, 108780,  
789 10.1016/j.soilbio.2022.108780, 2022

790 Gurung, R.B., Ogle, S.M., Breidt, F.J., Williams, S.A., and Parton, W.J.: Bayesian calibration of the DayCent  
791 ecosystem model to simulate soil organic carbon dynamics and reduce model uncertainty. *Geoderma*, **376**,  
792 114529, 10.1016/j.geoderma.2020.114529, 2020

793 Hartig, F., Minunno, F., Paul, S., Cameron, D., Ott, T., and Pichler, M.: BayesianTools: General-Purpose  
794 MCMC and SMC Samples and Tools for Bayesian Statistics. R package version 0.1.8, [https://CRAN.R-](https://CRAN.R-project.org/package=BayesianTools)  
795 [project.org/package=BayesianTools](https://CRAN.R-project.org/package=BayesianTools) (last access: 2 May 2025), 2019.

796 Harmon, M. E., Moreno, A., and Domingo, J. B.: Effects of partial harvest on the carbon stores in Douglas-  
797 fir/western hemlock forests: a simulation study. *Ecosystems*, **12**, 777-791, 2009

798 Hawkins, H.-J., Cargill, R.I.M., Van Nuland, M.E., Hagen, S.C., Field, K.J., Sheldrake, M., Soudzilovskaia,  
799 N.A., and Kiers, E.T.: Mycorrhizal mycelium as a global carbon pool. *Current Biology*, **33(11)**, R560-R573,  
800 2023

- 801 Heuvelink, G.B.M., Angelini, M.E., Poggio, L., Bai, Z., Batjes, N.H., van den Bosch, R., Bossio, D., Estella, S.,  
802 Lehmann, J., Olmedo, G.F., and Sanderman, J.: Machine learning in space and time for modelling soil organic  
803 carbon change. *Eur J Soil Sci*, **72(4)**, 1607-1623, 2021
- 804 Huang, X.-Y., Xiao, Q., Barker, D.M., Zhang, X., Michalakes, J., Huang, W., Henderson, T., Bray, J., Chen, Y.,  
805 Ma, Z., Dudhia, J., Guo, Y., Zhang, X., Won, D.-J., Lin, H.-C., and Kuo, Y.-H.: Four-dimensional Variational  
806 Data Assimilation for WRF: Formulation and Preliminary Results. *Mon Weather Rev*, 137(1), 299-314,  
807 [10.1175/2008MWR2577.1](https://doi.org/10.1175/2008MWR2577.1), 2009
- 808 Jevon, F.V., Polussa, A., Lang, A.K., Munger, J.W., Wood, S.A., Wieder, W.R., and Bradford, M.A.: Patterns  
809 and controls of aboveground litter inputs to temperate forests. *Biogeochemistry*, **161**, 335-352, 2022
- 810 Lavallee, J.M., Soong, J.L., and Cotrufo, M.F.: Conceptualizing soil organic matter into particulate and mineral-  
811 associated forms to address global change in the 21<sup>st</sup> century. *Glob Change Biol*, **26(1)**, 261-273,  
812 [10.1111/gcb.14859](https://doi.org/10.1111/gcb.14859), 2020
- 813 Le Dimet, F., and Talagrand, O.: Variational algorithms for analysis and assimilation of meteorological  
814 observations: Theoretic aspects. *Tellus*, **38A**, 97-110, 1986
- 815 Leuthold, S.J., Haddix, M.L., Lavallee, J., and Cotrufo, M.F.: Physical fractioning techniques. *Encyclopedia of*  
816 *Soils in the Environment*, 2, 68-80, [10.1016/B978-0-12-822974-3.00067-7](https://doi.org/10.1016/B978-0-12-822974-3.00067-7), 2023
- 817 Liu, C., Xiao, Q. and Wang, B.: An Ensemble-Based Four-Dimensional Variational Data Assimilation Scheme.  
818 Part I: Technical Formulation and Preliminary Test. *Mon Weather Rev*, **136(9)**, 3363-3373,  
819 [10.1175/2008MWR2312.1](https://doi.org/10.1175/2008MWR2312.1), 2008
- 820 Lorenc, A.C., Ballard, S.P., Bell, R.S., Ingleby, N.B., Andrews, P.L.F., Barker, D.M., Bray, J.R., Clayton, A.M.,  
821 Dalby, T., Li, D., Payne, T.J., and Saunders, F.W.: The Met Office global three-dimensional variational data  
822 assimilation scheme. *Quarterly J Royal Meteorol Soc*, **126(570)**, 2991-3012, 2000
- 823 Loria, N., Lai, R., and Chandra, R.: Handheld In Situ Methods for Soil Organic Carbon Assessment.  
824 *Sustainability*, **16(13)**, 5592, 2024
- 825 Lugato, E., Lavallee, J.M., Haddix, M.L., Panaganos, P., and Cotrufo, M.F.: Different climate sensitivity of  
826 particulate and mineral-associated soil organic matter. *Nature Geoscience*, **14(5)**, 295-300, 2021
- 827 Luo, Z., Viscarra-Rossel, R.A., and Qian, T.: Similar importance of edaphic and climate factors for controlling  
828 soil organic carbon stocks of the world. *Biogeosciences*, **18(6)**, 10.5194/bg-18-2063-2021, 2021
- 829 Marschmann, G.L., Pagel, H., Kugler, P., and Streck, T.: Equifinality, sloppiness, and emergent structures of  
830 mechanistic soil biochemical models. *Environ Model Softw*, **122**, 104518, [10.1016/j.envsoft.2019.104518](https://doi.org/10.1016/j.envsoft.2019.104518), 2019
- 831 Mathers, C., Black, C.K., Segal, B.D., Gurung, R.B., Zhang, Y., Easter, M.J., Williams, S., Motew, M.,  
832 Campbell, E.E., Brummit, C.D., Paustian, K., and Kumar, A.A.: Validating DayCent-CR for cropland soil  
833 carbon offset reporting at a national scale. *Geoderma*, **438**, 116647, [10.1016/j.geoderma.2023.116647](https://doi.org/10.1016/j.geoderma.2023.116647), 2023
- 834 Matthews, E.: Global litter production, pools, and turnover times: Estimates from measurement data and  
835 regression models. *J Geophys Res Atmos*, **102(D15)**, 18771-18800, 1997
- 836 Nemo, Klumpp, K., Coleman, K., Dondini, M., Goulding, K., Hasting, A., Jones, M.B., Leifeld, J., Osborne, B.,  
837 Saunders, M., Scott, T., Teh, Y.A., and Smith, P.: Soil Organic Carbon (SOC) Equilibrium and Model  
838 Initialisation Methods: an Application to the Rothamsted Carbon (RothC) Model. *Environ Model Assess*, **22**,  
839 215-229, 2017
- 840 Orgiazzi, A., Ballabio, C., Panagos, P., Jones, A., and Fernande-Ugalde, O.: LUCAS soil, the largest expandable  
841 soil dataset for Europe: a review. *Eur J Soil Sci*, **69**, 140-153, 2018
- 842 Papaioannou, I., Betz, W., Zwirgmaier, K., and Straub, D.: MCMC algorithms for subset  
843 simulation. *Probabilistic Eng Mech*, **41**, 89-103, 2015
- 844 Peylin, P., Bacour, C., MacBean, N., Leonard, S., Rayner, P., Kuppel, S., Koffi, E., Kane, A., Maignan, F.,  
845 Chevallier, F., Ciais, P., and Prunet, P.: A new stepwise carbon cycle data assimilation system using multiple

846 data streams to constrain the simulated land surface carbon cycle. *Geosci Model Dev*, **9**, 3321-3346,  
847 10.5194/gmd-9-3321-2016, 2016

848 Pierson, D., Lohse, K.A., Wieder, W.R., Patton, N.R., Facer, J., de Graaff, M.-A., Georgiou, K., Seyfried, M.S.,  
849 Flerchinger, G., and Will, R.: Optimizing process-based models to predict current and future soil organic carbon  
850 stocks at high-resolution. *Sci Rep*, **12**, 10824, 2022

851 Pinnington, E.M., Casella, E., Dance, S.L., Lawless, A.S., Morison, J.I., Nichols, N.K., Wilkinson, M. and  
852 Quaife, T.L.: Investigating the role of prior and observation error correlations in improving a model forecast of  
853 forest carbon balance using Four-dimensional Variational data assimilation. *Agric For Meteorol*, **228**, 299-314,  
854 2016

855 Pinnington, E., Quaife, T., Lawless, A., Williams, K., Arkebauer, T., and Scoby, D.: The Land Variational  
856 Ensemble Data Assimilation Framework: LAVENDAR v1.0.0. *Geosci Model Dev*, **13**, 55-69, 10.5194/gmd-13-  
857 55-2020, 2020

858 Pinnington, E., Amezcua, J., Cooper, E., Dadson, S., Ellis, R., Peng, J., Robinson, E., Morrison, R., Osborne, S.,  
859 and Quaife, T.: Improving soil moisture prediction of a high-resolution land surface model by parameterising  
860 pedotransfer function through assimilation of SMAP satellite data. *Hydrol Earth Sys Sci*, **25(3)**, 1617-1641,  
861 10.5194/hess-25-1617-2021, 2021

862 Quaife, T.: C implementation of 4DnEnVar using the GSL. Github repository,  
863 [https://github.com/tquaife/4DnEnVar\\_engine](https://github.com/tquaife/4DnEnVar_engine), 2023

864 Raczka, B., Hoar, T.J., Duarte, H.F., Fox, A.M., Anderson, J.L., Bowling, D.R., and Lin, J.C.: Improving  
865 CLM5.0 Biomass and Carbon Exchange Across the Western United States Using a Data Assimilation System. *J*  
866 *Adv Model Earth Sys*, e2020MS002421, [10.1029/2020MS002421](https://doi.org/10.1029/2020MS002421), 2021

867 Raoult, N.M., Jupp, T.E, Cox, P.M., and Luke, C.M.: Land-surface parameter optimisation using data  
868 assimilation techniques: the adJULES system v1.0. *Geosci Model Dev*, **9**, 2833-2852, 10.5194/gmd-9-2833-  
869 2016, 2016

870 Raoult, N., Douglas, N., MacBean, N., Kolassa, J., Quaife, T., Roberts, A.G., et al.: Parameter estimation in land  
871 surface models: Challenges and opportunities with data assimilation and machine learning. *J Adv Model Earth*  
872 *Sys*, **17**, e2024MS004733, [10.1029/2024MS004733](https://doi.org/10.1029/2024MS004733), 2025

873 Robertson, A.D., Paustian, K., Ogle, S., Wallenstein, M.D., Lugato, E., and Cotrufo, M.F.: Unifying soil organic  
874 matter formation and persistence frameworks: the MEMS model. *Biogeosciences*, **16**, 1225-1248, 10.5194/bg-  
875 16-1225-2019, 2019

876 Roy, V.: Convergence diagnostics for markov chain monte carlo. *Annu Rev Stat Appl*, **7(1)**, 387-412, 2020

877 Ruder, S.: An overview of gradient descent optimization algorithms. *arXiv preprint arXiv:1609.04747*, 2016

878 Rumpel, C., Amiraslani, F., Chenu, C., Cardenas, M.G., Kaonga, M., Koutika, L.-S., Ladha, J., Madari, B.,  
879 Shirato, Y., Smith, P., Soudi, B., Soussana, J.-F., Whitehead, D., and Wollenberg, E.: The 4p1000 initiative:  
880 opportunities, limitations and challenges for implementing soil organic carbon sequestration as a sustainable  
881 development strategy. *Ambio*, **49(1)**, 350-360, 10.1007/s13280-019-01165-2, 2020

882 Running, S.W., Nemani, R.R., Heinsch, F.A., Zhao, M., Reeves, M., and Hashimoto, H.: A continuous satellite-  
883 derived measure of global terrestrial production. *BioScience*, **54**, 547-560, 2004

884 Saito, K., and Nakano, R.: Partial BFGS update and efficient step-length calculation for three-layer neural  
885 network. *Neural computation*, **9(1)**, 123-141, 1997

886 Scharlemann, J.P.W., Tanner, E.V.J., Hiederer, R., and Kapos, V.: Global soil carbon: understanding the largest  
887 terrestrial carbon pool. *Carbon Manag*, **5**, 81-91, [doi.org/10.4155/cmt.13.77](https://doi.org/10.4155/cmt.13.77), 2014

888 Schlamadinger, B., Bird, N., Johns, T., Brown, S., Canadell, J., Ciccacese, L., Dutschke, M., Fiedler, J.,  
889 Fischlin, A., Fearnside, P., Corner, F., Freibauer, A., Frumhoff, P., Hoehne, N., Kirschbaum, M.U.F., Labat, A.,  
890 Marland, G., Michaelowa, A., Montanarella, L., Moutinho, P., Murdiyarso, D., Pena, N., Pingoud, K.,

891 Rakonczay, Z., Rametsteiner, E., Rock, J., Sanz, M.J., Schneider, U.A., Shvidenko, A., Skutsch, M., Smith, P.,  
892 Somogyi, Z., Trines, E., Ward, M., and Yamagata, Y.: A synopsis of land use, land-use change and forestry  
893 (LULUCF) under the Kyoto Protocol and Marrakech Accords. *Environ Sci Policy*, **10(4)**, 271-282, 2007

894 Schrumpf, M., Kaiser, K., Guggenberger, G., Persson, T., Kogel-Knabner, I., and Schulze, E.-D.: Storage and  
895 stability of organic carbon in soils as related to depth, occlusion with aggregates, and attachment to minerals.  
896 *Biogeosciences*, **10**, 1675-1691, 10.5194/bg-10-1675-2013, 2013

897 Sierra, C.A., Malghani, S., and Muller, M.: Model structure and parameter identification of soil organic matter  
898 models. *Soil Biol Biochem*, **90**, 197-203, [10.1016/j.soilbio.2015.08.012](https://doi.org/10.1016/j.soilbio.2015.08.012), 2015

899 Smith, P., Soussana, J.-F., Angers, D., Schipper, L., Chenu, C., Rasse, D.P., Batjes, N.H., van Egmond, F.,  
900 McNeill, S., Kuhnert, M., Arias-Navarro, C., Olesen, J.E., Chirinda, N., Fornara, D., Wollenberg, E., Alvaro-  
901 Fuentes, J., Sanz-Cobena, A., and Klumpp, K.: How to measure, report and verify soil carbon change to realize  
902 the potential of soil carbon sequestration for atmospheric greenhouse gas removal. *Glob Change Biol*, **26(1)**,  
903 219-241, 2020

904 Sokol, N.W., Whalen, E.D., Jilling, A., Kallenbach, C., Pett-Ridge, J., and Georgiou, K.: Global distribution,  
905 formation and fate of mineral-associated soil organic matter under changing climate: A trait-based perspective.  
906 *Funct Ecol*, **36(6)**, 1411-1429, 10.1111/1365-2435.14040, 2022

907 ter Braak, C.J.F., and Vrugt, J.A.: Differential evolution Markov chain with snooker updater and fewer chains.  
908 *Stat Comput*, **18**, 435e446, 10.1007/s11222-008-9104-9, 2008

909 Thepaut, J.N., and Courtier, P.: Four-dimensional variational data assimilation using the adjoint of a multilevel  
910 primitive-equation model. *Quarterly J Royal Meteorol Soc*, **117(502)**, 1225-1254, 1991

911 Tippett, M.K., Anderson, J.L., Bishop, C.K., Hamill, T.M.,

912 Tuomi, M., Thum, T., Jarvinen, H., Fronzek, S., Berg, B., Harmon, M., Trofymow, J.A., Sevanto, S., and Liski,  
913 J.: Leaf litter decomposition – Estimates of global variability based on the Yasso07 model. *Ecol Modell*, **220**,  
914 3362-3371, 10.1016/j.ecolmodel.2009.05.016, 2009

915 van den Berg, N.J., van Soest, H.L., Hof, A.F., den Elzen, M.G.J., van Vuuren, D.P., Chen, W., Drouet, L.,  
916 Emmerling, J., Fujimori, S., Hoehne, N., Koberle, A.C., McCollum, D., Schaeffer, R., Shekhar, S.,  
917 Vishwanathan, S.S., Vrontisi, Z., and Blok, K.: Implications of various effort-sharing approaches for national  
918 carbon budgets and emission pathways. *Clim Change*, **162**, 1805-1822, 2020

919 Viskari, T., Pusa, J., Fer, I., Repo, A., Vira, J., and Liski, J.: Calibrating the soil organic carbon model Yasso20  
920 with multiple datasets. *Geosci Model Dev*, **15(4)**, 1735-1752, 10.5194/gmd-15-1735-2022, 2022

921 Viskari, T., Quaipe, F., Fahl, F., Zhang, Y., and Lugato, E.: Comparing the MEMS v1 model performance with  
922 MCMC and 4DEnVar calibration methods over a continental soil inventory,  
923 <https://doi.org/10.5281/zenodo.17314989>, (Last accessed October 10 2025), 2025

924 Vrugt, J.A.: Markov chain Monte Carlo simulation using theDream software package: Theory, concepts, and  
925 MATLAB implementation. *Environ Model Softw*, **75**, 273-316, 10.1016/j.envsoft.2015.08.013, 2016

926 Wieder, W. R., Grandy, A. S., Kallenbach, C. M., and Bonan, G. B.: Integrating microbial physiology and  
927 physio-chemical principles in soils with the MIcrobial-MIneral Carbon Stabilization (MIMICS)  
928 model. *Biogeosciences*, **11(14)**, 3899-3917, 2014

929 Yu, W., Huang, W., Weintraub-Leff, S.R., and Hall, S.J.: Where and why do particulate organic matter (POM)  
930 and mineral-associated organic matter (MAOM) differ among diverse soils? *Soil Biol Biochem*, **172**, 108756,  
931 2022